NOAA Technical Memorandum ERL NSSL-71

INTERACTION OF TWO CONVECTIVE SCALES WITHIN A SEVERE THUNDERSTORM: A CASE STUDY

and

THUNDERSTORM WAKE VORTEX STRUCTURE AND AERODYNAMIC ORIGIN

Leslie R. Lemon

National Severe Storms Laboratory
Norman, Oklahoma
June 1974

Property of
NWC Library
University of Oklahoma

UNITED STATES
DEPARTMENT OF COMMERCE
Frederick B. Dent, Secretary

NATIONAL OCEANIC AND
ATMOSPHERIC ADMINISTRATION
Robert M. White, Administrator

Environmental Research
Laboratories
Wilmot N. Hess, Director

ACKNOWLEDGMENTS

The author expresses his sincere appreciation to Dr. Stanley Barnes for guidance, encouragement, suggestions, and editorial assistance during this study. Dr. Edwin Kessler also improved the report by his editorial counsel.

The comments and suggestions of Dr. Robert Davies-Jones and my colleagues of the Morphology and Dynamics Project were enlightening and most helpful. Thanks also go to Helen Ardrey for styling, to Charles Clark and Jennifer Fa for superior graphics work, to Brenda Courtney for patience and quality in manuscript typing and to Jim Henderson and Mike Weible for data processing assistance. I also wish to thank Kenneth Wilk under whose supervision the work was begun.

TABLE OF CONTENTS

	Page
ACKNOWLEDGMENTS	ii
LIST OF FIGURES	vi
INTERACTION OF TWO CONVECTIVE SCALES WITHIN A SEVERE THUNDERSTORM: A CASE STUDY	
ABSTRACT	
1. INTRODUCTION	1
2. SYNOPTIC SITUATION	1
3. INSTRUMENTATION AND DATA HANDLING	2
4. STORM HISTORY	3
5. RADAR ECHO CHARACTERISTICS	3
5.1 Supercell Structure	6
5.2 Storm Motion	6
5.3 Multi-cell Structure	6
6. SURFACE WEATHER	7
6.1 Surface Discontinuities	7
6.1.1 Wind Shift Line	11
6.1.2 Surge Line	11
6.1.3 Mesoscale Cold Occlusion	11
6.1.4 Gust Front	11
6.2 Mesocyclone	11
6.3 Pressure	12
6.4 Divergence	13
7. CELL MERGER WITH SUPERCELL	14
8. CONCLUSIONS	14
9. REFERENCES	14

TABLE OF CONTENTS

	Page
THUNDERSTORM WAKE VORTEX STRUCTURE AND AERODYNAMIC ORIGIN	
ABSTRACT	17
1. INTRODUCTION	17
2. RADAR DATA ANALYSIS	18
3. SURFACE DATA ANALYSIS	20
3.1 Wind	20
3.2 Divergence	20
3.3 Pressure	20
3.4 Wet-bulb Potential Temperature	20
4. VORTEX ORIGIN	23
4.1 Kármán Vortices	23
4.2 Starting Vortex Hypothesis	24
5. CONCLUSIONS	26
6. REFERENCES	27
APPENDIX A: OBJECTIVE SURFACE AND RADAR ANALYSES	30
APPENDIX B: SURFACE DATA GRAPHS	36
APPENDIX C: OTHER WAKE VORTEX OCCURRENCES	42

LIST OF FIGURES

INTERACTION OF TWO CONVECTIVE SCALES WITHIN A SEVERE THUNDERSTORM: A CASE STUDY

Figure		Page
1	Hodograph of Tinker AFB rawinsonde winds for 0600 CST 25 June 1969.	2
2	NSSL 1969 surface mesonetwork station locations with 20 km radar range marks. The mesh size of the surface analysis grid is also shown.	2
3	CAPPI radar displays for 1 km elevation, obtained from digital radar data. A few representative network stations are marked and surface wind field discontinuities included.	4
4	Mean wind velocity and direction, and cell paths relative to surface network.	7
5	Objectively analyzed streamlines and isotachs.	8
6	Surface composite analyses.	9
7	Time versus objectively analyzed surface values of: minimum pressure of supercell associated mesodepression, maximum convergence, and planimeter determined areal coverage within -1.5×10^{-3} sec^{-1} convergence contour.	12

THUNDERSTORM WAKE VORTEX STRUCTURE AND AERODYNAMIC ORIGIN

1	WSR-57 log contour displays 25 June 1969 showing stages of wake eddy development.	19
2	Pressure and divergence contours relative to 1 km elevation radar echo.	21
3	Wet-bulb potential temperature maximum relative to 1 km elevation radar echo.	22
4	Schematic diagram of a Kármán vortex forming downstream of the updraft in mid-level ambient flow with accompanying downdraft.	24

Figure		Page
5	Schematic diagram of "starting vortex" formation to updraft lee embedded in mid-level ambient flow and accompanying downdraft.	25

APPENDIX C

C1	WSR-57 integrated log contour displays of eddy-shedding storms.	43

INTERACTION OF TWO CONVECTIVE SCALES WITHIN A SEVERE THUNDERSTORM: A CASE STUDY

Leslie R. Lemon

National Severe Storms Laboratory
Norman, Oklahoma 73069

Detailed surface and radar data show an organized persistent severe thunderstorm that blends elements of the classic supercell (Browning and Donaldson, 1963) and the multi-cell storm (Marwitz, 1972). Changes of supercell strength reflect the contributions of cells from a flanking line that overtake and combine with the main storm. One cell led to deepening the storm mesodepression and increasing surface convergence as it merged with the supercell weak echo (updraft) region. Cells move both to the right and left as well as with the mean winds. Surface data reveal a large persistent mesodepression, associated convergence area and one principal downdraft along with smaller mesohighs and accompanying divergence regions.

1. INTRODUCTION

The Thunderstorm Project results (Byers and Braham, 1949) show thunderstorms to be groups of convective cells (updraft-downdraft couplets), each a few kilometers in diameter. Browning and Ludlam (1962) and Browning and Donaldson (1963) developed the concept of a large quasi-steady supercell, typically 20 km to 50 km in diameter. The squall line, another basic storm type, is a lateral alignment of persistent cells (Newton, 1963 and others). Marwitz (1972) proposed a classification system that included storms in an environment of strong vertical wind shear, where one large cell changes steadily by periodic discrete propagation on the front flank.

This study of a storm on 25 June 1969 reveals two interacting convective scales within a strongly sheared environment. The storm blends the multi-cell and supercell types while propagating both discretely and continuously. Radar and surface data show small and large convection scales and their interactions.

2. SYNOPTIC SITUATION

Jessup (1972) considered the synoptic situation. In general, thunderstorms were prefrontal with a low-level, warm, very moist layer (wet-bulb potential temperature $\sim$ 26C, dewpoint $\sim$ 30C). The Lifted Index was -6 and the average vector shear (850 to 100 mb) in the cloud-bearing layer was 6.5 x 10^{-3} sec^{-1}, as taken by 0600 and 1800 CST soundings from Tinker Air Force Base

18 km northeast of the radar site at NSSL headquarters. The 0600 hodograph (Fig. 1) indicates strong low-level veering, a low-level jet, and upper tropo spheric flow of about 30 m sec^{-1}.

3. INSTRUMENTATION AND DATA HANDLING

The NSSL mesonetwork (Fig. 2) during 1969 storm observations averaged 11 km spacing between stations which recorded surface wind speed and directio barometric pressure, relative humidity, temperature, and rainfall. See Sanders (1965) for complete instrumentation, calibration, recording, and data sorting techniques used in network operations.

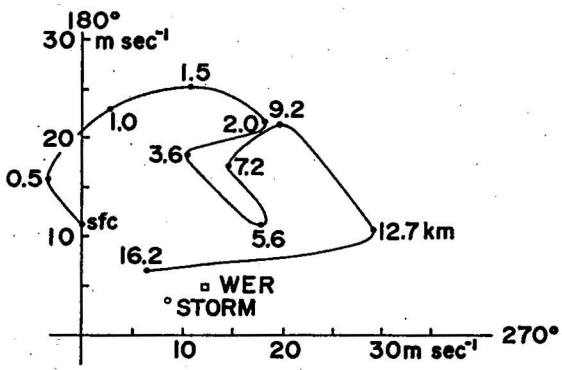

Figure 1. Hodograph of Tinker AFB rawinsonde winds for 0600 CST, 25 June 1969. Motions of storm and weak echo region (WER) are included.

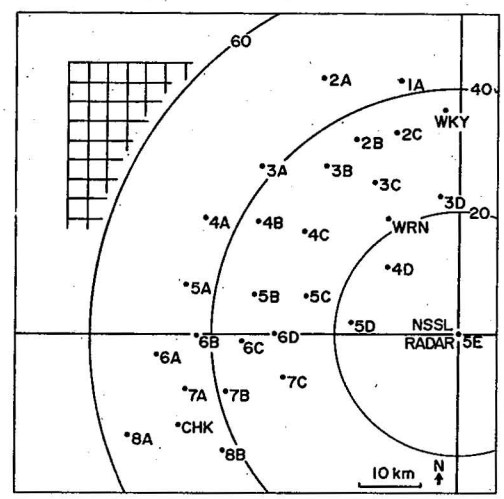

Figure 2. NSSL 1969 surface mesonetwork station locations with 20 km radar range marks. The mesh size (3.175 km) of the surface analysis grid is shown in the upper left corner.

Surface data from 1530 to 1830 (all times are CST) on 25 June were reduced and systematic errors removed by use of each station's calibration records. Uncertainties of $\pm$ 22.5° in instantaneous wind direction were reduced through 5-min averaging and smoothing. Individual station biases in pressure are eliminated by referencing pressure deviations to individual 3-hr linear trends determined by regression analysis.

Our objective analysis uses asynoptic data and has been described by Barnes (1973). Data consisting of wind speed and direction, divergence, vorticity, temperature, relative humidity, wet-bulb potential temperature, and pressure are analyzed on a 3.175 km grid. Significant features are compared with radar echoes.

The NSSL WSR-57 10-cm radar with a 2° conical beam width was used with an antenna scan rate of 1.5 rpm. The WSR-57 return signal, processed and recorded on magnetic tape, was displayed remotely as described by Wilk and Kessler (1968) and Sirmans et al. (1970). Range-height data were also recorded from a 4.7 cm MPS-4 radar with a 1.4° conical beam width. During each scan, 35-mm cameras automatically photographed both radar displays. Digital WSR-57 radar data were taken as the storm moved across the network while the antenna was continuously cycling in elevation from 1° to 4° (at 1° intervals). The data were converted to a CAPPI presentation (Henderson, 1972), at intervals of 1 km from 1 to 4 km above the terrain. Then CAPPI displays were contoured and transferred to network base maps.

4. STORM HISTORY

Lemon (1970) and Jessup (1972) briefly discuss the storm's behavior and path from its inception at 1455 until it began moving into the network around 1600. It first moved with the mean flow in the cloud bearing layer, which was from 227° at about 24 m sec^{-1}. As the storm moved into the network, it slowed and turned to the right. The storm complex as a whole moved from 248° at 9 m sec^{-1} through the network while the weak echo region (WER) moved from about 248° at 13 m sec^{-1}.

The first hail reported by cooperative observers occurred at 1545 and the last occurred at about 1945. Reports of 3 to 4 cm diameter hail were common, with the average size 1.5 cm and largest 5 cm. Reports of National Weather Service, Air Force, cooperative observers, Storm Data, and radar data, indicate that the storm produced hail nearly continuously.

The author first clearly viewed cloud base beneath the WER around 1640 to 1645. Organized cyclonic circulation was then observed, with cloud base estimated at 1 km above the terrain. Around 1700 to 1705 a funnel cloud formed above the thunderstorm's cold air outflow, with the funnel's lowest portion extending below 500 m. At 1707, station 5D recorded a sharp pressure dip of 3.8 mb and wind gusts of 35 m sec^{-1} as the funnel passed near the station.

5. RADAR ECHO CHARACTERISTICS

Pertinent features of the radar echo from 1616 through 1700 are shown for the 1 km level at 5-min intervals by contoured CAPPI displays, derived from processed digital radar data (Fig. 3). One prominent feature in the echo series (see especially 1630) is the apparent anticyclonic lee eddy which emerges from the echo and moves away. Both structure and physical implications are considered in the second paper in this technical memorandum.

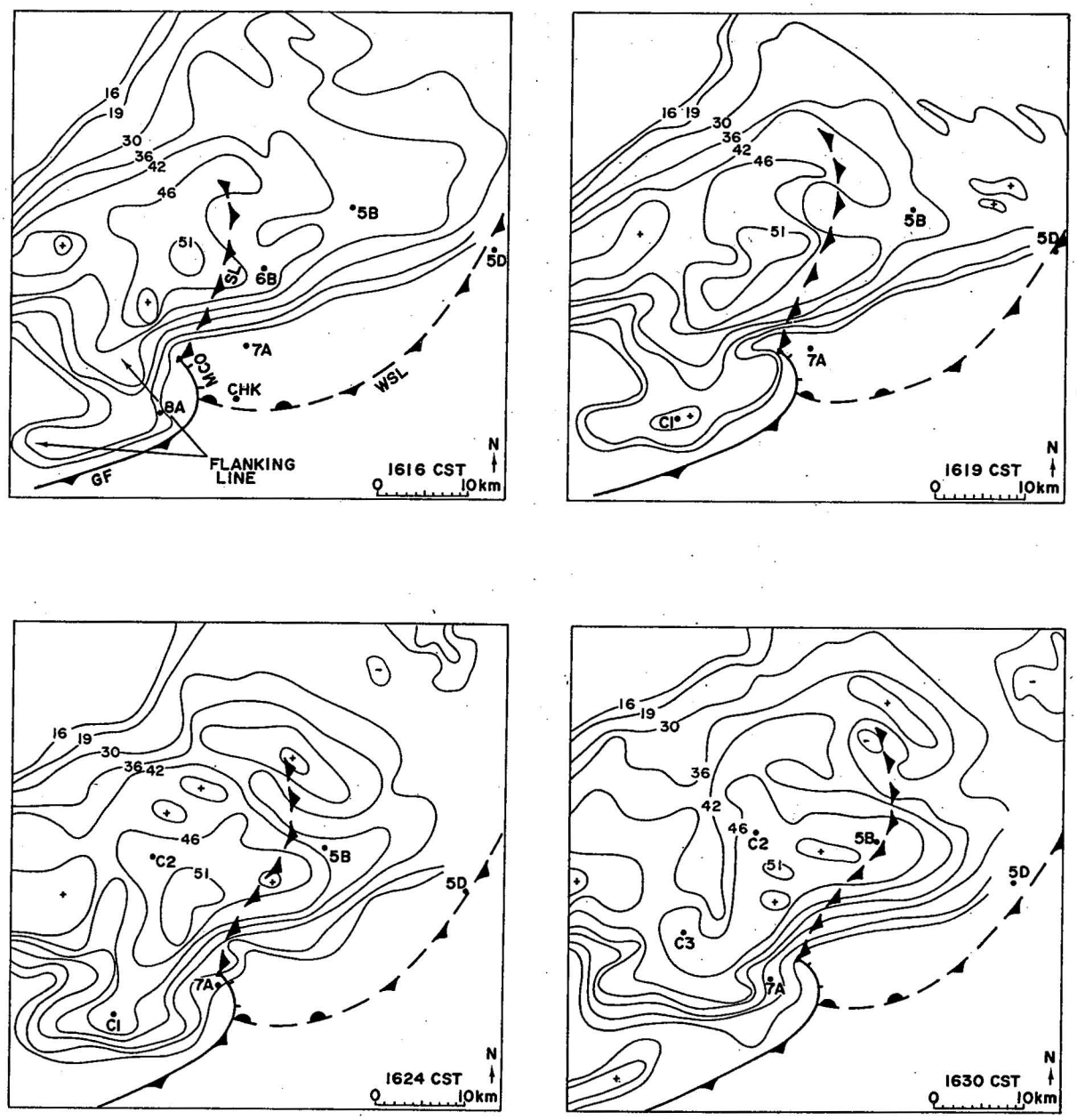

Figure 3. CAPPI radar displays for 1 km elevation, obtained from digital radar data. Reflectivity contour values are in dBZ. Unlabeled reflectivity maxima are indicated by (+) and minima by (-). A few representative network stations are marked. Surface wind field discontinuities are labeled at 1616; WSL--wind shift line, SL--surge line, MCO--mesoscale cold occlusion and GF--gust front. Small darkened triangle at juncture of SL and MCO indicates the wave crest. Cells are indicated by C1, C2, C3, C4, and two high reflectivity cores by CR1 and CR2. Analysis features are discussed on page 11.

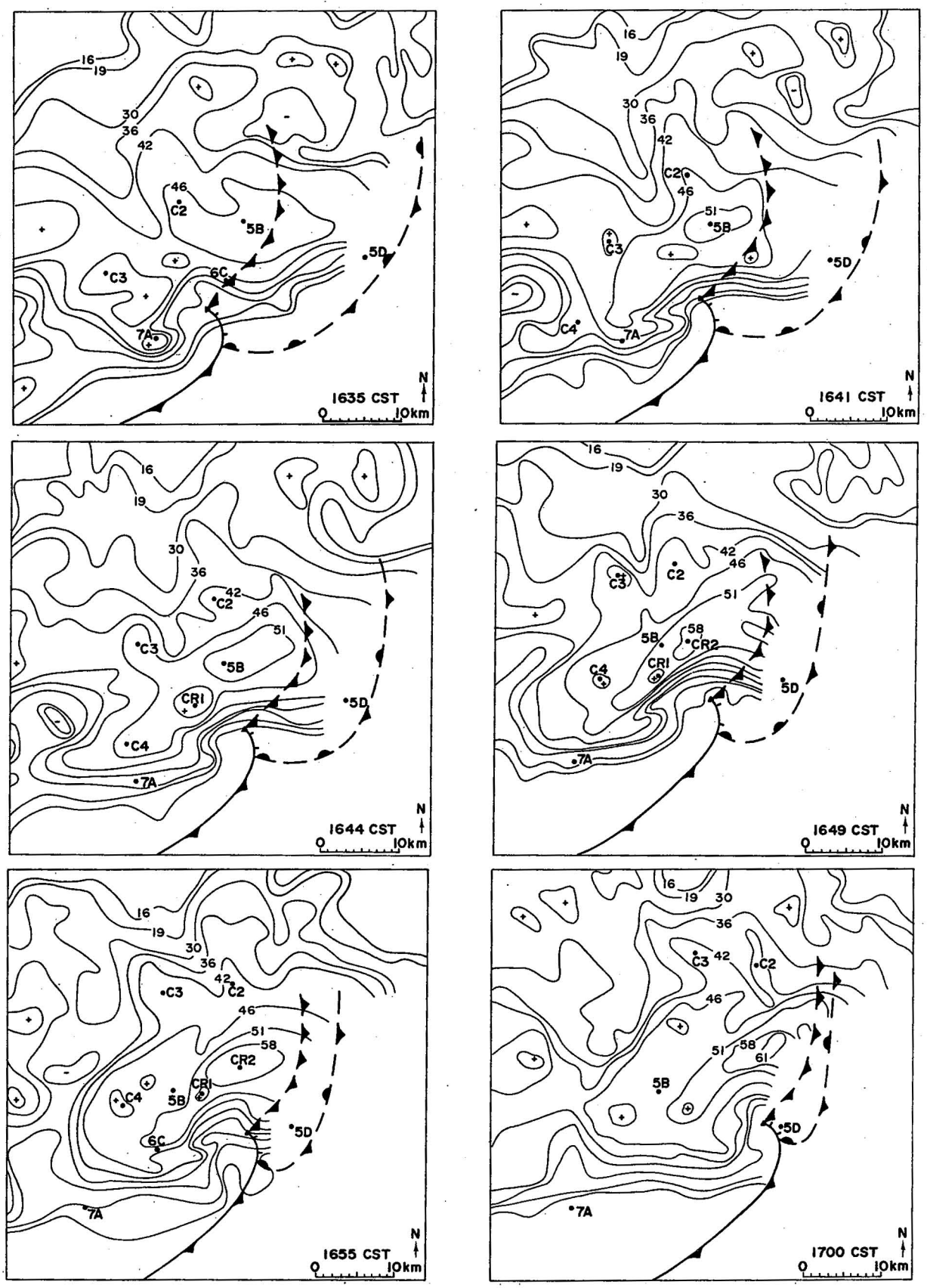

Figure 3 Continued

At 1616 there are two adjoining echo reflectivity masses exceeding 46 dBZ. The first is centered 8 km west of station 6B and is the core of the storm under study. The second area, or storm, is centered 15 km west of the first.

5.1 Supercell Structure

This storm maintained the supercell structure (Browning and Donaldson, 1963 and Browning, 1964) as shown by Lemon (1970), including a large weak echo region (WER) and a smaller, narrower structure within the WER (the vault) where updraft is believed to be strongest. Above the vault the storm also maintained one maximum echo top at 18.5 km through the analysis period as indicated by the Oklahoma City National Weather Service WSR-57 radar. Data from the MPS-4 radar indicated an average diameter of 16 to 18 km where the echo top emerged at a height of 9.5 km from surrounding echo.

The distinctive supercell feature is the hook appendage, which developed at the 1 km level at 1630, 3 km west of station 7A in the 42 dBZ contour (see Fig. 3). The hook moved from 246° at 13 m sec^{-1} (with the WER) and was tracked into the radar ground clutter after 1700. Between 1 and 2 km levels, it was tilted 53° from the vertical in a south-to-north slope.

5.2 Storm Motion

Marwitz (1972) established that at least one primary source for rightward motion of supercells is continuous propagation. While new updraft forms on the right WER side, old updraft dissipates on the left. The 25 June storm moved through the network 21° right of the mean winds. Discrete propagation occurred between 1616 and 1644 as developing cells in a line on the right rear flank merged with the storm. This process is detailed in the next section. From 1644 through 1700 the storm also moved to the right, although discrete propagation was not observed. Continuous propagation might explain the rightward motion. A complicating factor of thunderstorm rotation exists in this case. Fujita (1965), Goldman (1966), and Charba and Sasaki (1968) have proposed the Magnus effect to explain storms deviating to the right of the mean winds. A contribution from this force may have been realized.

5.3 Multi-cell Structure

Unlike supercell storms synthesized to date, this storm propagated <u>discretely</u> during part of its supercell stage. At 1616 (Fig. 3) an echo band extends southward about 13 km south-southwest of the storm's core turning near station 8A more westward. The cellular nature of the echo line is found at higher levels (not shown). The line lies parallel and behind the advancing gust front and was probably initiated by the discontinuity. The echo band called a "flanking line," projects more directly westward between 1635 and 1644. Henderson (1968) states that this structure represents major storm inflow and is quite common in single cell storms. Dennis et al. (1970) described the flanking line as "feeder clouds." The author, observing this area visually about 1615 to 1620, noticed a line of rapidly growing cumulus merging with the main cumulonimbus from the southwest.

Echo segments identified as cells are so named because: (1) the echo segment is resolvable with height in the form of a reflectivity core (or tower on the RHI radar), and/or (2) the echo segment's general structure and movement do not change with time. Intermittent RHI data show cell tops of 10 to 13 km. Where the cells rise above surrounding echo they are 2 to 6 km in diameter, or nearly an order of magnitude smaller than the major storm top. Three identifiable cells develop within the flanking line and overtake the storm, merging with or moving through the storm echo. Origin of the remaining cells is uncertain. Two high reflectivity cores (CR1 and CR2) persist at the 1 km level and are trackable. Unlike those commonly associated with the cell complex (Marwitz, 1972; Chisholm and Renick, 1972) the centroids of cells move with varying directions and speeds, e.g., 214° at 18 m sec^{-1} to 243° at 19 m sec^{-1} (Fig. 4).

Cells C2, C3 and C4 (Fig. 3, 1624-1700) although moving unusually, develop like those in other multi-cell storms: development on the right rear flank, movement with the storm and dissipation on the left flank. These cells had little effect other than propagation on the supercell structure.

The area a few kilometers north of the WER where reflectivity cores CR1 and CR2 developed (Fig. 3, 1644-1700) is commonly a hail area in supercells. Observers and other surface reports verify that these cores contain large hail. They are probably hail shafts as opposed to updraft-downdraft couplets, and therefore a consequence of the supercell structure.

Cell C1 is easily identified at the 1 km level only between 1619 and 1624 as it moves from the flanking line (Fig. 3). Afterward, at both 1 km and higher levels, the cell merges with surrounding echo at the WER edge and can no longer be identified. Surface data indicate that C1 has an important impact on the supercell updraft.

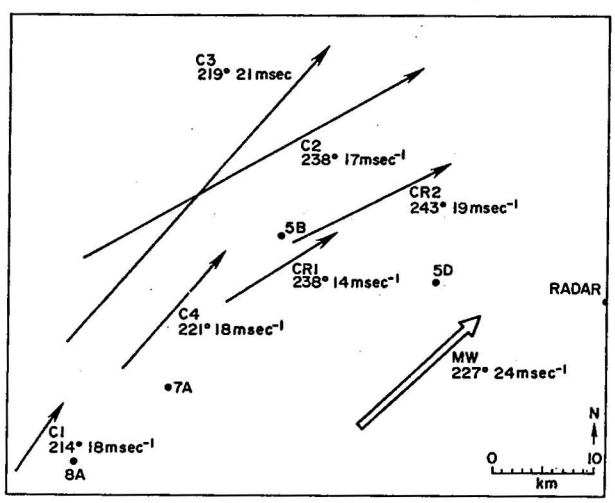

Figure 4. Mean wind (MW) velocity and direction, and cell paths relative to surface network.

6. SURFACE WEATHER

This section treats wind (related gust fronts, convergence and divergence), pressure, and wet-bulb potential temperatures (θ_w) and their relationships to radar echo structure. Objective analyses of these fields from 1615 to 1700 are shown in Appendix A.

6.1 Surface Discontinuities

A distinctive arrangement of meteorological discontinuities is associated with the storm's surface structure. These discontinuities are described briefly below. General characteristics are illustrated in Figs. 3, 5 and 6. The reader may refer for details to Appendices A and B.

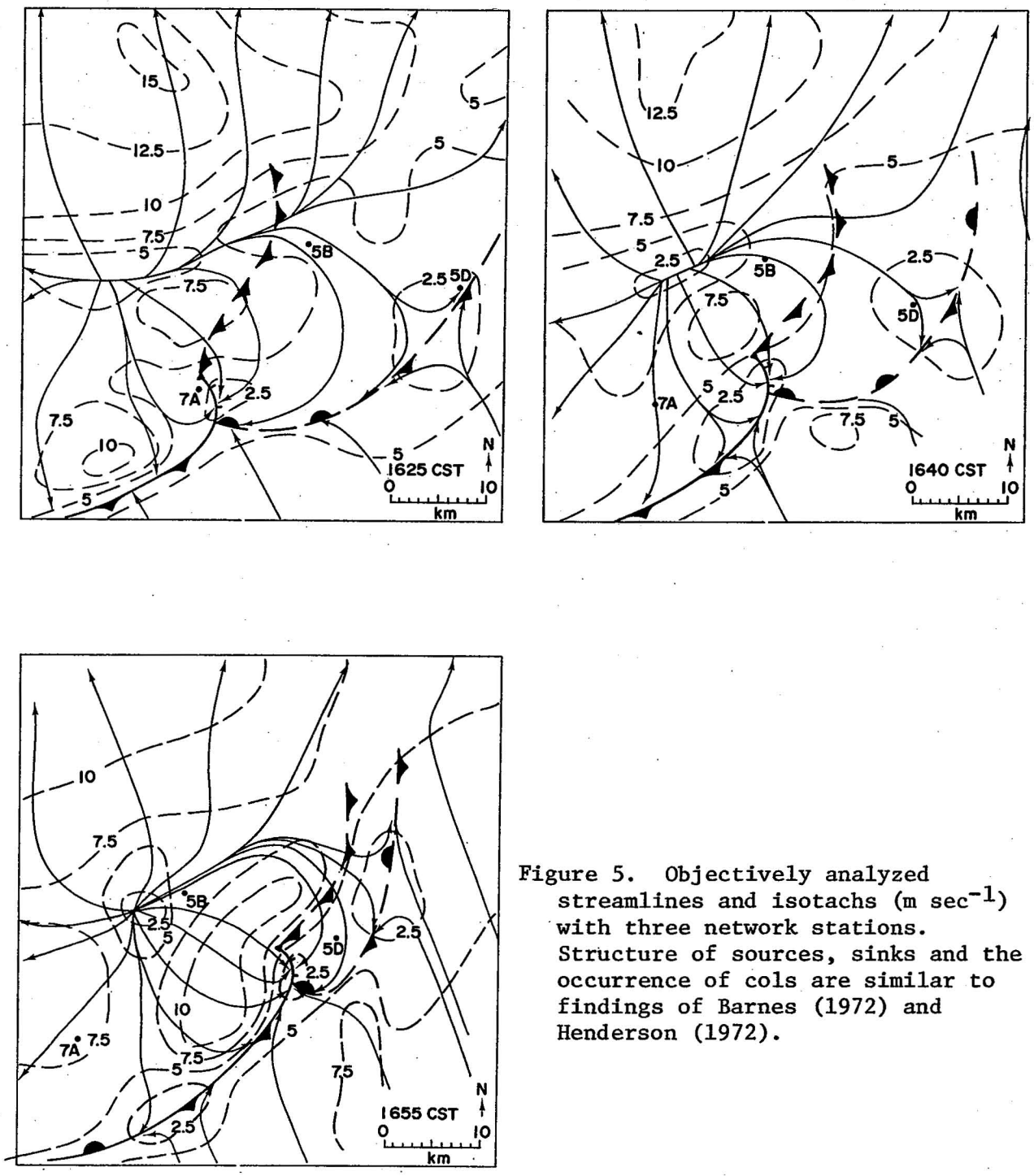

Figure 5. Objectively analyzed streamlines and isotachs (m sec^{-1}) with three network stations. Structure of sources, sinks and the occurrence of cols are similar to findings of Barnes (1972) and Henderson (1972).

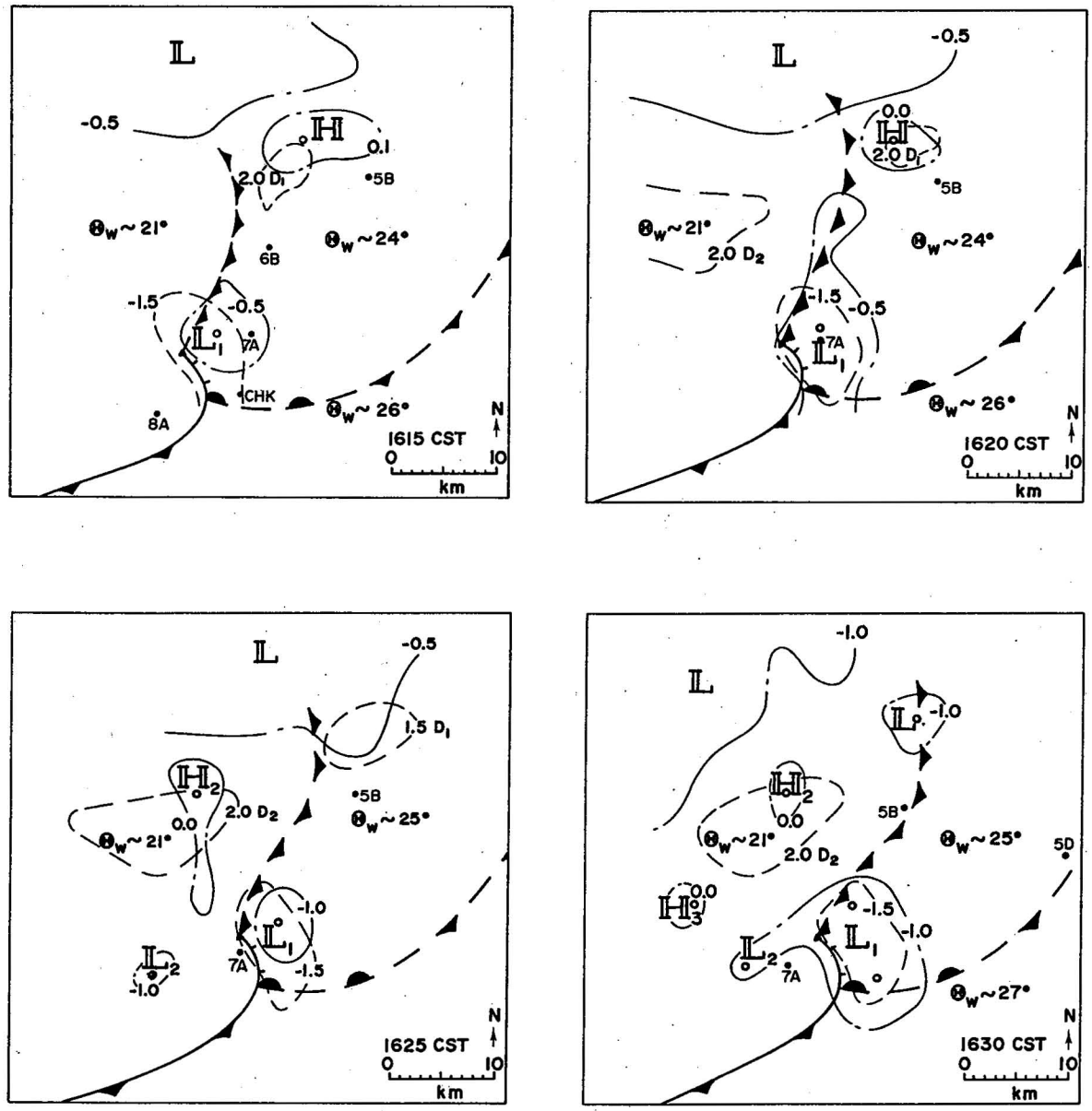

Figure 6. Surface composite analyses. Included are: wind field discontinuities (as in Fig. 3); pressure excess contours in mb (—— - ——); pressure center locations (open dot); divergence (x 10^{-3} sec^{-1}) regions (---), with negative values indicating convergence; wet-bulb potential temperature values (θ_wC). D_1 and D_2 identify specific divergence regions. Various station locations are marked (as in Fig. 2).

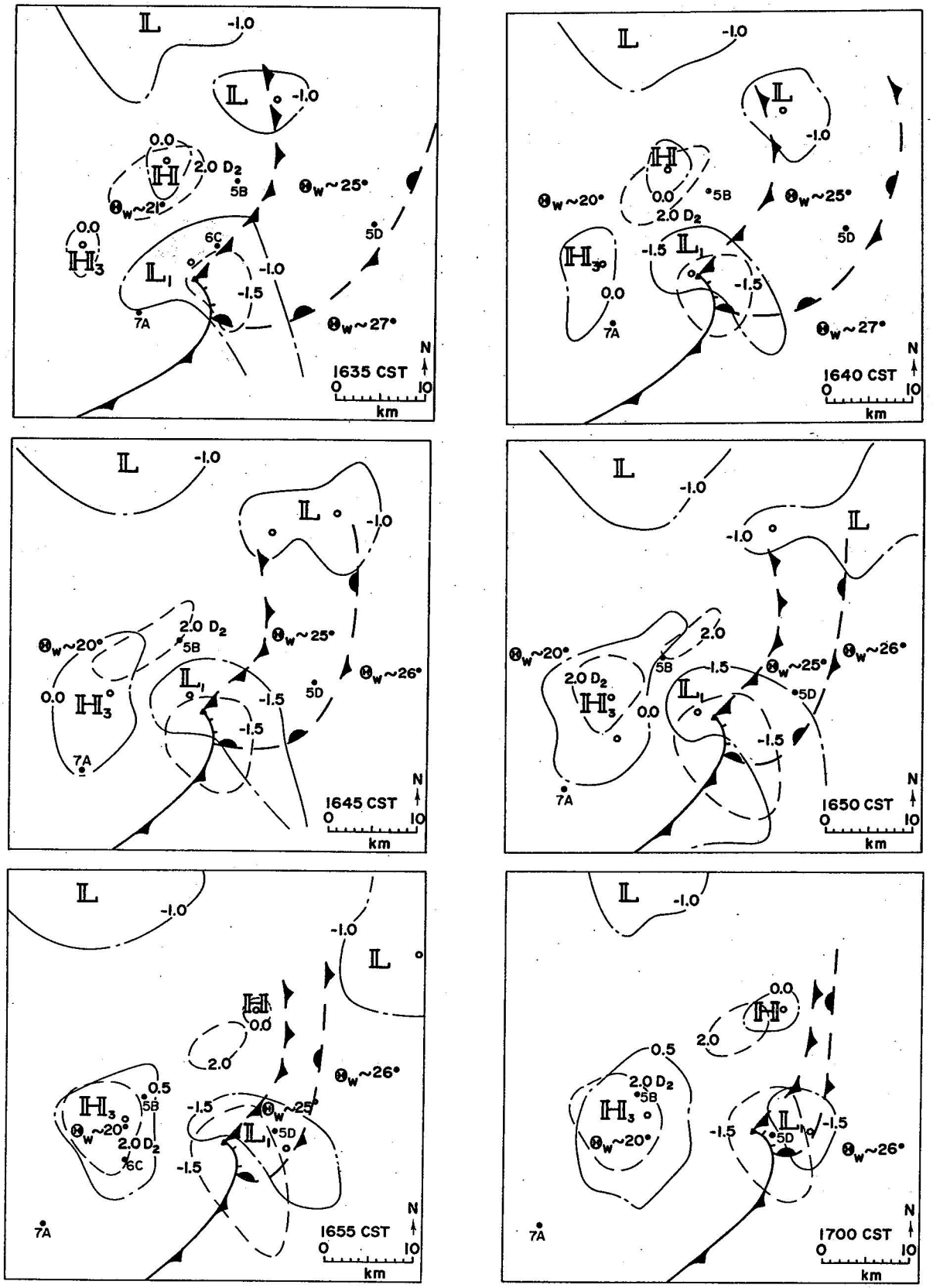

Figure 6 Continued

6.1.1 Wind Shift Line

A moderate thunderstorm moving through the network between 1430 and 1545 produced the wind shift line, or WSL (Fig. 3, 1616). The leading outflow edge (often termed "first gust" or "gust front") advanced over nearly all the northern and western network portions by 1600. Continued slow eastward motion is marked by a wind shift from southerly to southwest or west, minor speed change, unchanged or slight pressure rises, and θ_w falls of 1 to 2C. By 1635 the discontinuity is quasi-stationary, along the eastern and southern portions of the network. It is apparently along this gust front southwest of the network that the major storm develops. Near the surface convergence area (broken warm front symbols, Fig. 3, 1616), the WSL returns north and northeastward. The existence of the WSL is apparently prolonged by divergence which occurs behind it in association with the major storm from 1615 through 1640.

6.1.2 Surge Line

The "surge line" (SL), part of one "thunderstorm scale" airmass interface, is embedded within a light precipitation region, and its passage is followed by an increase of wind speed and gustiness. Commonly, wind direction shifts only slightly (i.e., 0° to 30°) as the SL passes. High relative humidity 90% to 100% and a pressure trough further characterize the SL. Within a few minutes after passage of the surge line, θ_w drops sharply (3 to 5C).

6.1.3 Mesoscale Cold Occlusion

The second section of the joint discontinuity is labeled MCO or "mesoscale cold occlusion" because of the similarity of its location to the synoptic scale cold occlusion. The MCO differs markedly from the SL in that the wind direction shifts abruptly from northeast to southwest and its speed increases with MCO passage. As shown in Sections 6.3 and 6.4 the area a few kilometers ahead of the MCO is dominated by the storm mesodepression and surface roots of the supercell updraft. Inflow to this region originates from a moist rainy downdraft with θ_w values of 25 to 26C. Behind the MCO the surface is dominated by air with $\theta_w \sim$ 21C that has descended from mid-levels (deduced from 0600 to 1800 soundings).

6.1.4 Gust Front

The last discontinuity termed the "gust front" (GF) resembles the Colmer (1971) and Charba (1972) gust fronts. The pressure starts to rise a few minutes before the gust front passage, and the wind shift, gustiness and temperature break occur together as it passes. Winds shift from south-southeast to northwest, then gradually to the northeast. A warm, very moist air mass with θ_w values of 27C is found along and south of the GF at the roots of flanking line updraft.

6.2 Mesocyclone

One-minute wind data clearly show the presence of cyclonic circulation or a mesocyclone after 1640. Five-minute averaged data used in the analyses

portray only weak circulation, however. Location of the point sink or mesocyclone center in Fig. 5 is imprecise, but analog wind records and isochrone analysis show both circulation center and wave crest passed north of stations 7A and 5D and south of 6C and 6D. These data, coupled with wave crest configuration and evolution, indicate a coincident mesocyclone and crest.

6.3 Pressure

Surface pressure distribution is generally consistent with echo, discontinuity, and mesocyclone structures. Pressure contours (line-dot) and centers (open dots, extracted from analyses in Appendix A) relate to other surface features in Fig. 6 and can be compared to Fig. 3 for locations relative to the radar echo. Fig. 7a includes the objectively determined maximum pressure deficit of the major mesodepression (L_1) as a function of time.

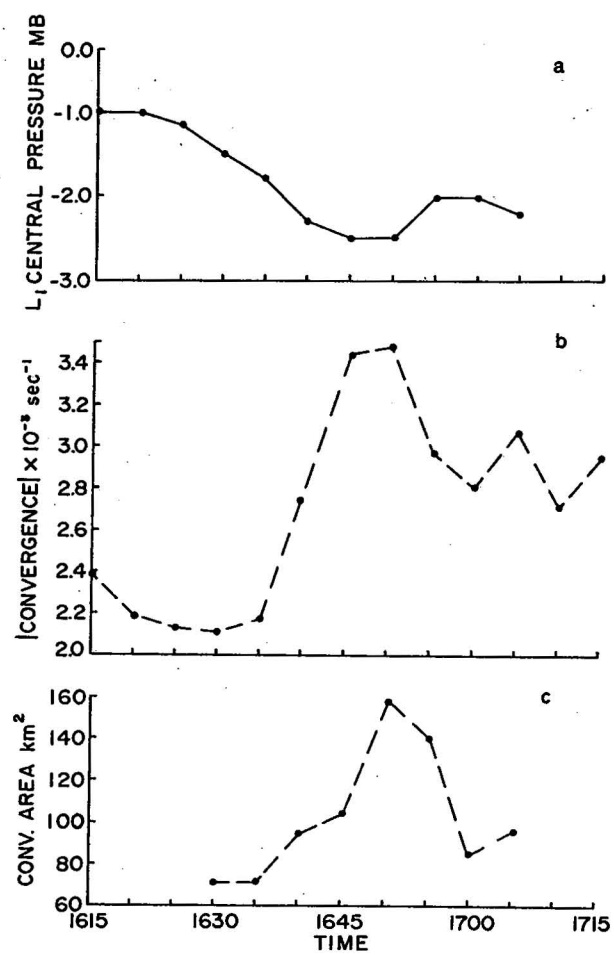

Figure 7. Time versus objectively analyzed surface values of: (a) minimum pressure of supercell associated mesodepression L_1, (b) maximum convergence associated with L_1, and (c) planimeter determined areal coverage within -1.5×10^{-3} sec^{-1} convergence contour.

Recently Barnes (1972) has presented evidence showing separation of the circulation center and mesodepression. This study reveals that, at the time of greatest pressure deficit (1640 to 1650), the lowest pressure is coincident with the circulation's center; at other times the circulation is apparently too weak to bring them into coincidence. Although the lowest pressure deficit (Fig. 7a) based on the objective analysis (with smoothing of data) is -2.5 mb, unsmoothed processed data indicate a low of at least -3.1 mb.

The effect of new cell merger with the supercell indicates a possible explanation for pressure center location shifting from east of the mesocyclone center to coincidence with it (Fig. 6, 1625-1640). At 1625, a second low, L_2, appears southwest of L_1, beneath echo C1. Low L_2 in cool surface air behind the GF most likely reflects the updraft belonging to C1. By 1630 the center of L_2 is beneath the newly developed hook echo, while a narrow pressure trough extends northeast and joins with depression L_1. At this time C1 can no longer be distinguished on radar. By 1640, L_2 is completely absorbed by L_1. From 1630 to 1635 the location (relative to the ground) of lowest pressure in L_1 remains unchanged while its location relative to the wave crest shifts from east to near the crest.

Moreover, two other events coincide with the merging process that occurs between 1625 and 1640. First, the edge of the 36 dBZ contour of the hook echo approaches the wave crest (Fig. 3). At 1624 the 36 dBZ contour edge in the area of hook echo formation 7 km from the wave crest, steadily approached the wave until 1641 when it was 4.5 km to the southwest. Second, pressure within L_1 lowers steadily and most rapidly during the merger of L_2 and L_1, reaching its lowest value from 1645 to 1650 (Fig. 7a). Pressure lowering within L_1 directly affects associated convergence (Section 6.4).

Mesohigh H_3 develops or is first detected at 1630 beneath C3. This excess-pressure region, associated with the precipitation core and downdraft, builds steadily and becomes the principal thunderstorm high. Central pressure excess values of 2.0 mb are reached shortly after 1700. Other smaller and less significant pressure centers also occur.

6.4 Divergence

The important convergence region (for strength and storm organization) is centered near the MCO, although some convergence is also characteristic of the other surface discontinuities. The convergence area (-1.5×10^{-3} sec^{-1}, Fig. 6) lies along and east of the MCO until 1640 when it becomes more symmetric about the line. The region moves with the storm WER, reaching maximum strength and greatest spatial coverage between 1645 and 1650 when surface pressure is lowest in mesodepression L_1 (see Fig. 7). The strengthening and increased coverage of convergence coincides with later merger stages of depressions L_2 and L_1, and the corresponding deepening of L_1.

Divergence region D_1 is relatively weak (2.3×10^{-3} sec^{-1}) and initially associated with the wake eddy and a rainy downdraft. It is important from two standpoints. The WSL existence is prolonged by rejuvenation of outflow behind it, and D_1 provides a warm nearly saturated surface air mass feeding the mesocyclone from the northeast. Region D_2 enters the network's west edge at 1620, and throughout the analysis associates with the principal downdraft

near the storm's rear edge. The region associated initially with a surface line source downdraft but gradually transposes to a point source by 1645 (see Fig. 5).

7. CELL MERGER WITH SUPERCELL

Streamlines coupled with θ_w fields (Appendix A) indicate that much surface mesocyclone inflow originated with divergence D_1. The potential temperature of supercell inflow averaged 2.4K less than in the air south of the GF in the source region for cell updrafts. One of the flanking line cells was entrained by the supercell updraft. The cell initially shielded the updraft from direct entrainment of dry mid-level ambient air approaching from the southwest. Three causes probably contributed to increased buoyancy and vertical acceleration of supercell updraft air: (a) increased volume of undiluted updraft air, (b) addition of warmer air from the smaller cell updraft, and (c) increased convergence at the surface in response to falling pressures in the mesocyclone. Increased vorticity convergence may also have enhanced updraft rotation, which would have further increased low-level convergence and decreased mid-level entrainment, as shown by Ward (1967). The overall effect of cell merger with the supercell is increased upward velocity (and possibly rotation as evidenced by hook echo formation) in the supercell, bringing decreased surface pressure and increased surface convergence.

8. CONCLUSIONS

A proper storm classification system will include supercell storms with flanking lines. NSSL radar film and visual observations (Golden, 1972) indicate that supercell storms with accompanying flanking lines are common, often severe, and relatively long-lived in Oklahoma. Two notable examples are tornadic storms studied by Barnes (1973b) where surface structures included WSL dilatation type discontinuities in the surface mesocyclone vicinity, and flanking lines.

When entrained into the supercell updraft, cells within the flanking line increase surface convergence, thereby increasing vertical velocity, and sometimes initiating or amplifying rotation.

9. REFERENCES

Barnes, S. L., 1972: Morphology of two tornadic storms. Preprints of Papers, Fifteenth Conf. Radar Meteorology, Champaign-Urbana, Ill., Amer. Meteor. Soc., 69-76.

_____, 1973a: Mesoscale objective map analysis using weighted time series observations. NOAA Tech. Memo ERLTM-NSSL-62, National Severe Storms Laboratory, Norman, Oklahoma, 60 pp.

_____, 1973b: Radar-observed merger of twin hook echoes. Preprints of Papers, Eighth Conf. on Severe Local Storms, Denver, Colo., Amer. Meteor. Soc., 155-160.

Browning, K. A., 1964: Airflow and precipitation trajectories within severe local storms which travel to the right of the winds. J. Atmos. Sci., 4, 634-639.

_____, and R. J. Donaldson, Jr., 1963: Airflow and structure of a tornadic storm. J. Atmos. Sci., 20, 533-545.

_____, and F. H. Ludlam, 1962: Airflow in convective storms. Quart. J. Roy. Meteor. Soc., 88, 117-135.

Byers, H. R., and R. R. Braham, 1949: The Thunderstorm. Washington, D. C., U. S. Government Printing Office, 287 pp.

Charba, J., 1972: Gravity current model applied to analysis of squall-line gust front. NOAA Tech. Memo ERLTM-NSSL-61, National Severe Storms Laboratory, Norman, Oklahoma, 58 pp.

_____, and Y. Sasaki, 1968: Structure and movement of severe thunderstorms of 3 April 1964 as revealed from radar and surface mesonetwork data analysis. ESSA Tech. Memo ERLTM-NSSL-41, 47 pp.

Chisholm, A. J., and J. H. Renick, 1972: The kinematics of multi-cell and supercell Alberta hailstorms. Research Council of Alberta, Hail Studies Report 72-2, 24-31.

Colmer, M. J., 1971: On the character of thunderstorm gust fronts. Roy. Aircraft Est., Bedford, England, 11 pp.

Dennis, A. S., C. A. Schock and A. Koscielski, 1970: Characteristics of hailstorms of western South Dakota. J. Appl. Meteor., 9, 127-135.

Fujita, T., 1965: Formation and steering mechanisms of tornado cyclones and associated hook echoes. Mon. Wea. Rev., 93, 67-78.

Golden, J. H., 1972: The NSSL-Notre Dame Tornado Intercept Program, Spring 1972, Bull. Amer. Meteor. Soc., 53, 1178-1180.

Goldman, J. L., 1966: The role of the Kutta-Joukowski force in cloud systems with circulation. ESSA Tech. Note 48, NSSL-27, National Severe Storms Laboratory, Norman, Oklahoma 21-34.

Henderson, J. H., 1972: A detailed description of the structure of a thunderstorm. Preprints of Papers, Fifteenth Conf. Radar Meteorology, Champaign-Urbana, Illinois, Amer. Meteor. Soc., 61-68.

Henderson, T. J., 1968: 6000 thunderstorms and what they indicate. Proc., International Conf. on Cloud Physics., Toronto, Amer. Meteor. Soc., 555-558.

Jessup, E. A., 1972: Interpretations of chaff trajectories near a severe thunderstorm. Mon. Wea. Rev., 100, 653-661.

Lemon, L. R., 1970: Formation and emergence of an anticyclonic eddy within a severe thunderstorm as revealed by radar and surface data. Preprints of Papers, Fourteenth Conf. Radar Meteorology, Tucson, Arizona, Amer. Meteor. Soc., 323-328.

Marwitz, J. D., 1972: The structure and motion of severe hailstorms. Part III: Severely sheared storms. J. Appl. Meteor., 11, 189-201.

Newton, C. W., 1963: Dynamics of severe convective storms. Meteor. Monographs 5, No. 27, 33-58.

Sanders, L. D., 1965: NSSL mesoscale network of surface stations. ESSA Tech. Note 3, NSSL-24, National Severe Storms Laboratory, Norman, Oklahoma, 131-139.

Sirmans, D., W. L. Watts, and J. Horwedel, 1970: Weather radar signal processing and recording at the National Severe Storms Laboratory. IEEE Trans. Geosci. Electron., GE-8, 88-94.

U. S. Department of Commerce, 1969: Storm Data, 11, No. 6.

Ward, N. B., 1967: An effect of rotation on a buoyant convective column. Preprints of Papers, Fifth Conf. on Severe Local Storms, St. Louis, Missouri, Amer. Meteor. Soc., 368-373.

Wilk, K. E., and E. Kessler, 1968: Quantitative radar measurements of precipitation. Meteor. Monographs, 11, No. 33, 315-329.

THUNDERSTORM WAKE VORTEX STRUCTURE AND AERODYNAMIC ORIGIN

Leslie R. Lemon

National Severe Storms Laboratory
Norman, Oklahoma 73069

The radar and surface structure of a severe thunderstorm's wake vortex are examined. Two aerodynamic explanations for wake vortex formation are considered: Kármán vortices and starting vortices to the updraft lee. Kármán vortices would form, as do those observed, within the echo core at the updraft lee "edges" and move downstream with the ambient flow. However, in contrast to Kármán's theory, the radar reflectivity distributions are consistently anticyclonic. The starting vortex would develop during the transition of a thunderstorm updraft from a non-rotational to rotational state, as a vortex of comparable strength and opposite circulation. Four other thunderstorms also produced severe weather, increased intensity rapidly, and turned right or formed hook echoes contemporaneously with vortex shedding.

1. INTRODUCTION

In the past 15 years, abundant evidence and theoretical developments have shown that thunderstorms act to some extent as barriers to the ambient winds. After Byers (1942) suggested that a thunderstorm is analogous to a circular cylinder embedded in potential flow, Newton and Newton (1959) proposed that this condition arises from the vertical transport of low-level horizontal momentum by the updraft. Fankhauser (1968, 1971) concluded from aircraft measured winds and chaff trajectories that mature thunderstorms both ingest and divert mid-tropospheric ambient air. Brown et al. (1973), using Doppler radar, found that both the updraft and associated tornado cyclone circulation in a severe thunderstorm block the relative flow. These findings establish the diversion of mid-tropospheric air around storm updrafts and accompanying mesoscale circulations.

Lemon (1970) showed that wake eddies are occasionally shed from severe thunderstorm updrafts and can be detected in the accompanying radar echo. Jessup (1972) analyzed chaff trajectories around one of the same storms analyzed by Lemon and confirmed the presence of wake vortex circulation. The hypothesis that air columns may obstruct the flow sufficiently to shed vortices is supported by McMahon's et al. (1971) laboratory experiments revealing vortices shed from a turbulent jet exhausting into a cross wind.

This paper examines the surface structure of Lemon's wake vortex (1970) with a considerably refined objective analysis technique, and considers the physical explanation of such eddies. Three other wake eddy occurrences are compared with the primary case.

2. RADAR DATA ANALYSIS

Through synthesis of radar film data Lemon found that wake eddies develop in a systematic manner:

1. The eddy is first detected in thunderstorm mid levels at the lee core edge ($\sim$ 40 dBZ) through a finger-like intrusion of lower reflectivity echo from the echo's forward flank (Fig. 1a).

2. As entrainment of low reflectivity echo increases and curves anticyclonically, a semi-circular arc or crescent of higher reflectivity ($Z_e \geq 40$ dBZ) echo results north of the intrusion and joins the main storm echo at its left flank. This reflectivity signature moves somewhat to the left of the cell's high reflectivity core (Fig. 1b). The same sequence occurs at progressively lower altitudes.

3. Flow (identified by time-lapse radar film of crescent and intrusion) continues to converge anticyclonically toward the eddy center, while reflectivities weaken in crescent and intrusion as the eddy moves away from the main storm (Fig. 1c).

4. The intrusion often dissipates more rapidly than the crescent, leaving the echo crescent connected with the major parent echo only at the crescent base (Fig. 1d). Apparent circulation continues until the crescent echo also dissipates.

Analysis of digital radar data in CAPPI format for the 25 June 1969 storm has not added to these findings. However, digital data does provide accurate radar signature positioning with surface data. It also helps to identify changes in general storm characteristics during eddy shedding. One such change is a rapid increase in PPI echo intensity.

At 1610 (all times are CST), 5 min before the radar first indicates eddy formation, areal coverage of echo $\geq$ 52 dBZ is 4, 8, and 0 km^2 at the 1, 2 and 3 km levels, respectively. During the next 14 min, coverages increased to 24, 62, and 60 km^2, respectively. During this period there is also a gradual rightward turn in storm motion, first strong indications of hook echo formation and first 2.5 cm diameter hail.

Radar eddy motion is to the left of the storm. Eddy movement from 1615 through 1700 is from 230° at 20 m sec^{-1}, or nearly with the mean wind of 227° at 24 m sec^{-1}. Storm motion was 248° at 9 m sec^{-1}.

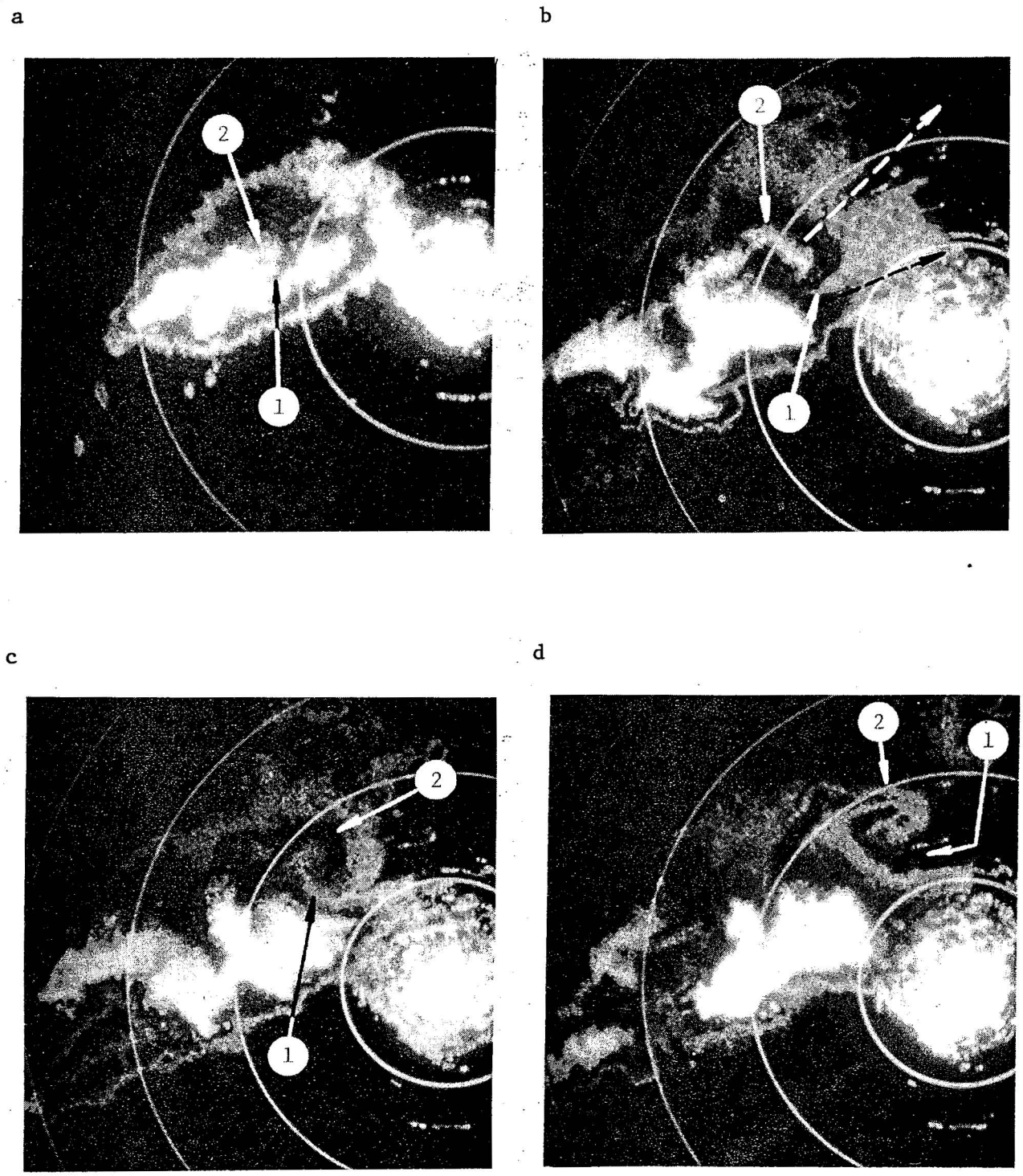

Figure 1. WSR-57 log contour displays 25 June 1969 showing stages of wake eddy development. Arrows indicate (1) low reflectivity intrusion, (2) high reflectivity crescent echo. In b, storm and eddy movement are also indicated by dashed arrows. Range marks are 20 nautical miles in a and 10 n mi in b, c, and d. Antenna elevation is 2° in each.

3. SURFACE DATA ANALYSIS

Surface mesonet observations are objectively analyzed (after Barnes, 1973) and related to flow and persistence of the wake vortex. Our new conclusions differ somewhat from earlier findings (Lemon, 1970).

3.1 Wind

While significant anticyclonic vorticity is not measured at the surface, some eddy effect is noted. Winds are predominantly southerly beneath the eddy radar signature (1624-1700) except during 1616-1624 when flow was divergent from westerly or northwesterly on the right eddy flank (relative to eddy motion) to southerly on the left flank.

The weakened eddy reflectivity structure passed over the 500 m WKY television tower meteorologically instrumented at six levels (Sanders and Webber, 1970). No discernible change in prevailing meteorological conditions was recorded by the facility during eddy passage (1655-1710). Lack of marked surface circulation is explained in section 4.

3.2 Divergence

From 1616 through about 1630, positive values of divergence dominated the eddy (Fig. 2). Rainfall rates, at station 5A, were 2.5 cm/hr beneath and near the eddy center between 1616 and 1619. These rates probably were creating subsidence from precipitation drag. Association of the eddy circulation and descending air near its center would help sustain or augment the circulation by vertical stretching. This effect must have been short-lived, however, since eddy-associated surface divergence became disorganized, weak, and apparently disassociated from the eddy by 1635.

3.3 Pressure

A small, weak pressure excess exists beneath the eddy crescent between 1616 and 1619 (Fig. 2). This is probably associated with high liquid water content aloft ($Z_e \geq 42$ dBZ) and an associated downdraft. By 1624, although weakening divergence still accompanies the eddy, the pressure excess is replaced by general lower pressure. At 1630, a closed pressure deficit (-1.0 mb) forms beneath the radar eddy center. Subsequently the small low moves northeastward more slowly than the eddy, remaining at its rear flank, while low pressure dominates the entire signature (Appendix A).

3.4 Wet-bulb Potential Temperature

Objective analyses of the θ_w field (Appendix A) reveal maximum values ($25C \leq \theta_w \leq 26C$) beneath the eddy. This air descended in the eddy-associated downdraft from 1616 to 1630, displacing 23C to 24C surface air from an old thunderstorm outflow region. This downdraft is unlike most others, which are characterized by lower θ_w. Rather distinct anticyclonic curvature of the region of maximum θ_w coincided well with the low reflectivity intrusion aloft from 1616 to 1630 (Fig. 3). The θ_w maximum subsequently moved with the eddy and merged with a second high θ_w region northeast.

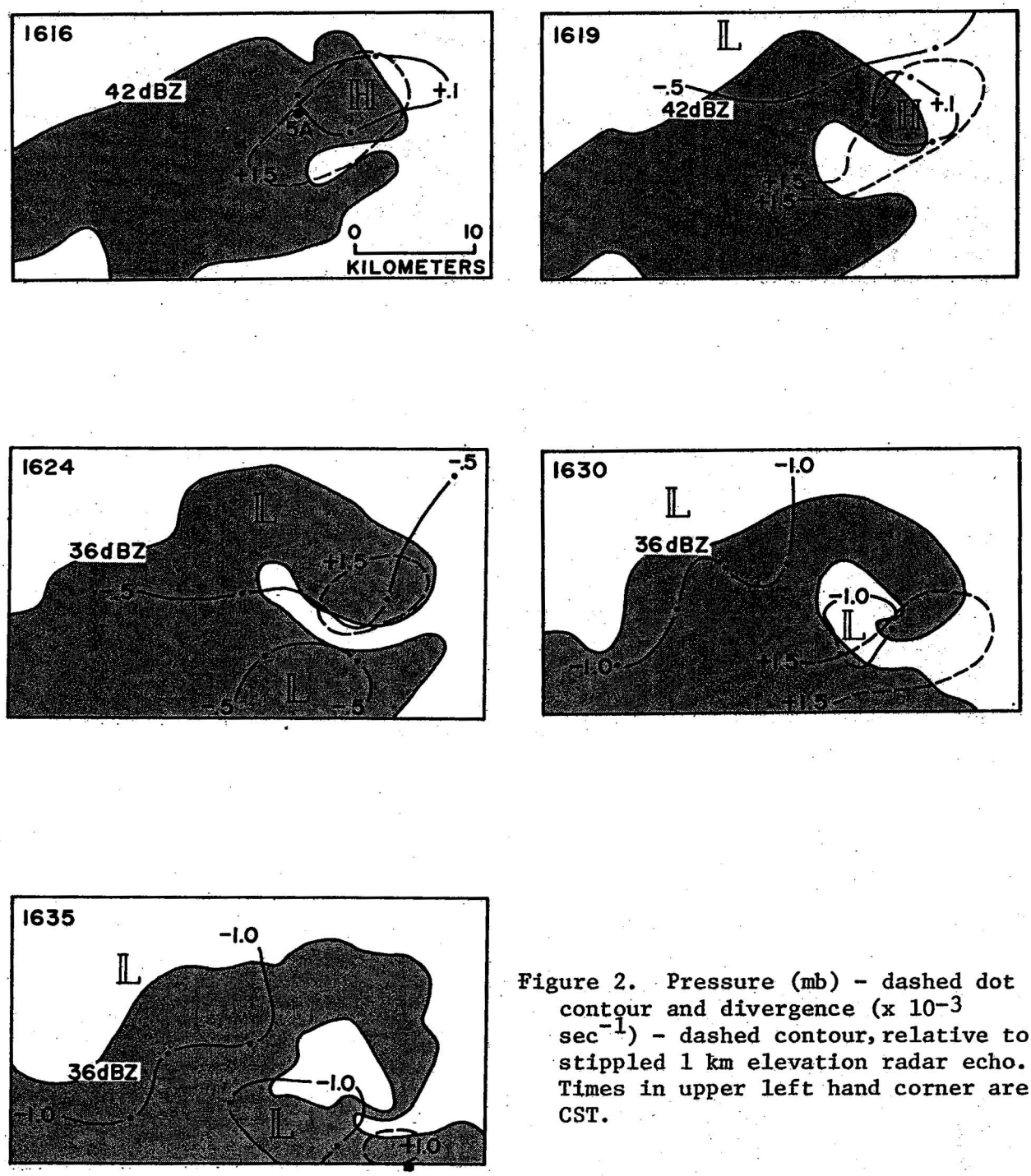

Figure 2. Pressure (mb) - dashed dot contour and divergence (x 10^{-3} sec^{-1}) - dashed contour, relative to stippled 1 km elevation radar echo. Times in upper left hand corner are CST.

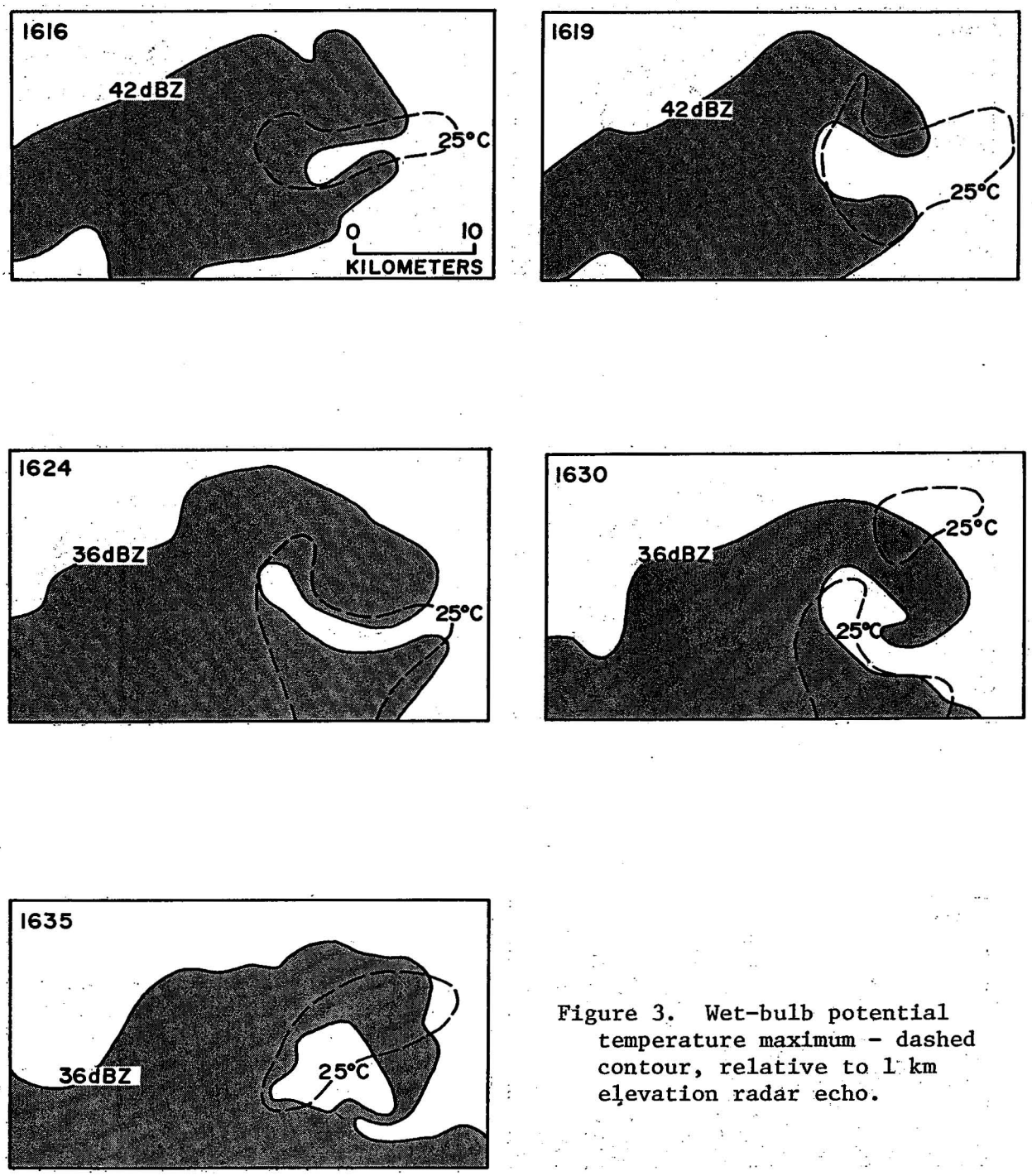

Figure 3. Wet-bulb potential temperature maximum - dashed contour, relative to 1 km elevation radar echo.

Why do the orientation and curvature of the surface θ_w maximum and eddy intrusion match so closely when there is no surface circulation? Rawinsonde soundings indicate that the air originates within 500 m of the surface. Near-surface air which encounters the wind shift line east of the circulation (see first paper) may be lifted and drawn into the eddy along the intrusion, forced downward again by the precipitation-induced downdraft, forming a surface band of relatively high θ_w air beneath the radar echo intrusion. Mid-level air (more commonly downdraft air) reaches the surface only along the crescent echo at the eddy signature's left flank (see Appendix A).

4. VORTEX ORIGIN

In recent years, studies by Burgess and Brown (1973), Fankhauser (1968), Fujita and Grandoso (1968), and Newton and Newton (1959) have shown that a thunderstorm acts somewhat as a barrier to the ambient mid-level wind flow. A wake to the lee of the barrier occurs naturally. Within laboratory-generated wakes, vortices of various types (standing, Kármán, starting, etc.) depend on critical flow and obstacle characteristics. Plausible explanations for the shedding of eddies from a blocking updraft are Kármán and "starting" vortices. We favor the latter for reasons given below.

4.1 Kármán Vortices

Existence of atmospheric Kármán vortices in the lee of islands has been shown by Chopra and Hubert (1965) and Zimmerman (1969). These vortices are shed from solid obstacles such as mountains. On the convective scale, Shmeter (1970) noted vortices during aircraft investigation of flow around cumulonimbi. He indicated that anticyclonic veer is usual at upper levels around the cloud, while windward to leeward wind velocity differs by as much as 30 m sec^{-1}. We have also referred to McMahon's (1971) study showing vortices shed from a turbulent jet in the laboratory.

If eddy vortices similar to the Kármán type are caused by a convective block, they should form within the echo core at the updraft lee "edges" and move downstream with the ambient flow (Fig. 4). Why then have only anti-cyclonic type eddies on the updraft left side been definitely identified to date? It may be that the right-hand Kármán vortices are suppressed by the heavier precipitation and associated rapid subsidence that characterizes the region at mid levels downstream of the updraft on the right side of the right-moving storms (Browning, 1964).

Eddies, detached from an obstacle, classically move downstream with the free stream flow (227°/24 m sec^{-1}). The observed eddy moved downstream from 230° at 20 m sec^{-1}. Rouse (1946) states that Kármán vortices move downstream at a velocity invariably less than the ambient fluid velocity, a fact possibly accounting for the 4 m sec^{-1} discrepancy.

Another question concerns lack of circulation at the surface or through the 500 m WKY tower depth. Barnett (1972) showed that vortices shed from islands occur between two inversions. The island penetrates both inversions, resulting in a flow around rather than over the blocking obstacle, creating lee vorticity concentrations and vortex streets. The upper boundary inversion prevents mixing between the vortex street and the layer above, and the lower

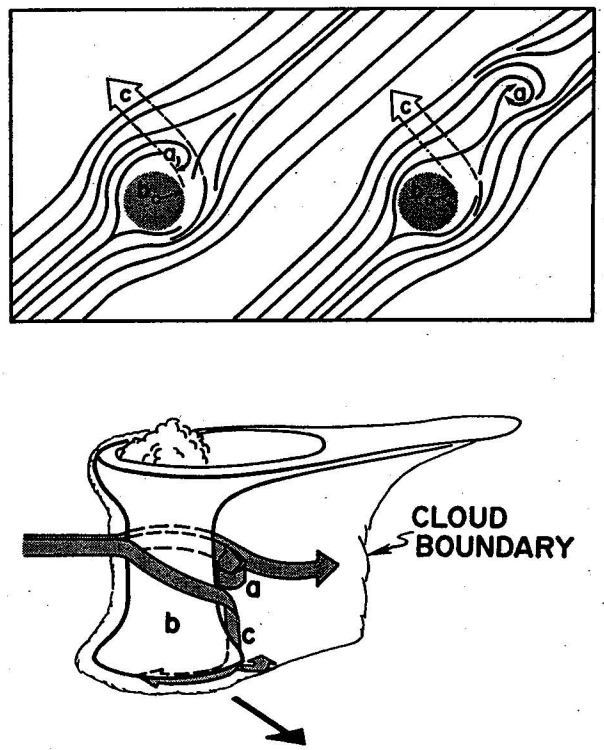

Figure 4. Kármán vortex (a) forming downstream of updraft (b), in mid-level ambient flow with accompanying downdraft, (c). Smaller arrow indicates updraft (and storm) movement.

inversion insulates the circulation from frictional dissipation effects of the earth's surface. Rawinsonde soundings (the last taken 18 km ahead of the storm's forward flank) on 25 June indicate a persistent low-level inversion between 1.5 and 2.4 km (MSL), and a nearly isothermal layer between 8.0 and 9.0 km. These inversions may explain the absence of surface circulation and the relatively long persistence of the eddy circulation aloft. The short-lived downdraft of limited size apparently lowered the low-level inversion temporarily. Low-level vorticity dispersion through mass divergence probably prevented a significant circulation from affecting the surface at that time. The presence of inversions in the immediate vicinity of the eddy cannot be verified.

Although some aspects of the Kármán theory appear reasonable, we must ask why eddy-shedding storms are infrequent. We also question why cyclonic shed vortices are not observed. A more physically consistent explanation of vortex origin may rest in the "starting vortex" theory.

4.2 Starting Vortex Hypothesis

Fujita (1965), Fujita and Grandoso (1968), Goldman (1966), and several others have suggested that the Magnus effect is at least partly responsible for convective storm motion to the right (or left) of the mean wind. The rotating cylinder hypothesis of these investigators could also account for the lee vortices on 25 June 1969 and at other times.

Prandtl and Tietjens (1934) demonstrated through filmed experiments that, during a cylinder's transition from a non-rotational to a rotational state, a vortex of comparable strength and opposite circulation to the cylinder forms and expands as it moves downstream with the free stream flow (Fig. 5). (The 25 June wake eddy diameter doubled from 5.6 to 12.4 km in 33 min.) The shed vortex seems to occur exclusively with severe storms. The concept of a starting vortex is directly supported by observations of vigorous updraft rotation in this storm and in those discussed in Appendix C. The strongest eddies should occur with severe storms since the strength of the wake vortex formed is comparable to updraft circulation strength. Wake vortex circulation on 25 June 1969 is approximately 3×10^5 m^2 sec^{-1} and is of the same order of magnitude as the tornado cyclone (5×10^5 m^2 sec^{-1}, Fujita, 1965). Wake circulation value is based on a tangential velocity of 10 m sec^{-1} determined

from the motion of small reflectivity perturbations along the crescent echo in the WSR-57 digital data. Further, the 25 June storm also underwent a gradual rightward turn during and following eddy shedding. The rightward storm motion attributed by some investigators to the Magnus force, occurs in theory only after the shedding of a starting vortex (Prandtl and Tietjens, 1934). In all cases, apparent cyclonic circulation was associated with the eddy shedding storms explaining the formation of only anticyclonic wake vortices.

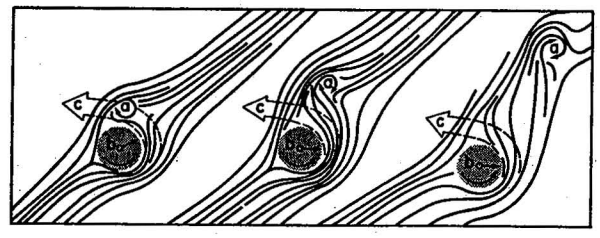

Figure 5. Formation of a "starting vortex" to the lee of an updraft. Updraft (b) begins and accelerates rotation. Starting vortex (a) moves downstream with ambient flow. The downdraft (c) exists in the updraft's wake. Small arrow shows increased rightward updraft movement.

Two storms apparently produced additional, although poorly defined, vortices. This does not alter the starting vortex hypothesis. The updraft's rotational character, being dependent on inflow vorticity, would likely vary. Thus, additional starting vortices could be produced as the updraft's rotational character changed through transient vorticity addition.

The previous discussion briefly mentions other eddy-producing thunderstorms (Appendix C). Five cases were observed at NSSL in 1969 and 1973. Closer examination of these storms supports the starting vortex hypothesis. Each storm underwent a right turn, formed a hook echo, or rapidly increased radar intensity contemporaneously with eddy formation. Intensity increase was indicated by rapid development or increase of a storm's reflectivity core. Ward (1967, 1968) concluded that updraft rotation augments buoyancy and enhances convection by decreasing mixing between buoyant and ambient air aloft. Thus, rapid increase in storm intensity may indicate transition from essentially non-rotating to a rotating updraft.

Since the Karman and "starting" vortex hypotheses depend on updraft blocking, it is not surprising to observe formation of all eddies at mid levels (6 to 8 km), where there is a minimum radial and a maximum vertical and tangential flow at the buoyant column periphery. Eddy formation would begin in an air sheath, resembling a boundary layer, which should form around the updraft, while below the level of nondivergence, convergence (or entrainment) into the updraft would remove the "boundary layer" air preventing vortex formation (Ewald et al., 1930). Scorer (1958) discusses prevention of free stream separation (and therefore eddy formation) by injection of fast moving fluid into the lee side boundary layer from within the obstruction. Such a process may be represented by strong outflow from severe storms at upper levels, with corresponding eddy prevention. Recent single Doppler data revealing strongest flow-around-an-obstacle signatures in mid levels is consistent with the above (Brown and Crawford, 1972; Burgess and Brown, 1973). Our observations of vortex descent may be attributed to precipitation drag and some evaporative cooling. During descent the circulation weakens, probably owing to diffusion of vorticity and lack of low level support and a temperature inversion characteristically prevents the vortex from reaching the surface.

Rawinsonde observations available for "eddy shedding" storms may indicate why most of those observed in Oklahoma occur during June. These soundings show the typical supercell environment (Marwitz, 1972): very moist, low-level unstable air with dry mid- and upper levels. However, relatively "light" winds at all levels (as often occur in June) are significantly different from typical spring soundings and appear to be favorable to vortex formation. Maximum winds in most cases are $\leq$ 32 m sec^{-1} and in all cases are between 26 m sec^{-1} and 31 m sec^{-1} at mid-levels. Prandtl and Tietjens (1934) show that starting vortices are shed within critical limits of the ratio of cylinder tangential and ambient free stream velocity. Similar atmospheric limits, although likely not the same as those found in the laboratory, are implied by the above rawinsonde observations for a convective blocking circulation and relative free stream flow.

That vortex shedding, as observed in a few cases, is not observed more frequently may be due to precipitation fallout before circulation becomes evident, or to eddy formation under a restricted range of ambient conditions relative to wind speeds, eddy viscosity, and Reynolds' numbers.

The previous discussion may suggest a relationship of splitting storms and wake vortices. However, surface and radar data indicate that an eddy can be considered passive, and any directly associated convection is relatively weak and short-lived. Two storms studied split into left- and right-moving counterparts approximately 30 min before wake vortex formation in the right-moving storm. Therefore, although at times both storm splitting and wake vortices occur during the severe storm's life, the generating mechanisms for these two phenomena are apparently different.

5. CONCLUSIONS

Abundant evidence indicates that anticyclonic wake vortices sometimes develop during severe weather events associated with convective storms. Surface and radar structure of the 25 June 1969 storm show that the eddy develops at mid levels and is transferred downward, but does not reach the surface. Inversions at upper and lower levels probably shield the vortex from destructive outflow effects above and from the earth's surface below.

Two aerodynamic explanations for vortex formation depend on the thunderstorm's updraft (and circulation) blocking character. The first explanation supposes that effective eddy viscosities and Reynold's numbers are in the proper range for Kármán vortex street formation. Then the lack of cyclonic wake eddies may be attributable in some way to the heavy precipitation that occurs to the right of the updraft as seen in the direction downstream along the mid-level flow.

We propose a "starting" vortex mechanism as a more promising explanation for wake eddy formation. This assumes that updraft rotation is variable and cyclonic in eddy-producing, right-moving severe thunderstorms. The environmental flow reacts to the updraft somewhat as a solid cylinder that begins or increases its rotation. This theory is supported by observations that storms increased intensity rapidly, turned right, and/or produced severe weather and

hook echoes contemporaneously with eddy formation. The theory also finds support (assuming rotating updrafts are most intense) in the occurrence of eddies with only those storms producing quite severe weather.

A limited data set indicates that these vortices are shed within a restricted range of environmental wind speeds. This implies wake vortex production in a narrow range of eddy viscosities and Reynolds' numbers.

Wake vortex formation is significant in three respects if the above findings can be documented in a larger number of storms. Whether the vortices are Kármán or starting vortices, the updraft blocking character would be confirmed in severe convective storms. If the "starting vortex" hypothesis is further supported, the Magnus force would be verified as a deflecting force in severe storm motion. Finally, recognition of anticyclonic vortex shedding on a PPI radar scope could be used as a severe weather indicator.

6. REFERENCES

Barnes, S. L., 1973: Mesoscale objective map analysis using weighted time series observations. NOAA Tech. Memo ERLTM-NSSL-62, National Severe Storms Laboratory, Norman, Oklahoma, 60 pp.

Barnett, K. M., 1972: A wind-tunnel experiment concerning atmospheric vortex streets. Boundary Layer Meteor., 2, 427-443.

Brown, R. A., D. W. Burgess and K. C. Crawford, 1973: Twin tornado cyclones within a severe thunderstorm: single-Doppler radar observations. Weatherwise, 26, 63-71.

Brown, R. A., and K.C. Crawford, 1972: Doppler radar evidence of severe storm high-reflectivity cores acting as obstacles to airflow. Preprints of papers, Fifteenth Conf. on Radar Meteo., Champaign-Urbana, Illinois, Amer. Meteor. Soc., 16-21.

Browning, K. A., 1964: Airflow and precipitation trajectories within severe local storms which travel to the right of the winds. J. Atmos. Sci., 4, 634-639.

Burgess, D. W. and R. A. Brown, 1973: The structure of a severe right-moving thunderstorm: new single-Doppler radar evidence. Preprints of Papers, Eighth Conf. on Severe Local Storms, Denver, Colorado, Amer. Meteor. Soc., 40-43.

Byers, H. R., 1942: Nonfrontal thunderstorms. Misc. Rep., No. 3, Meteor. Dept., Univ. of Chicago, 26 pp.

Chopra, K. P. and L. F. Hubert, 1965: Mesoscale eddies in wake of islands. J. Atmos. Sci., 22, 652-657.

Ewald, P.P., TH. Pöschl and L. Prandtl, 1930: The Physics of Solids and Fluids. Blackie and Son Limited, London, 363 pp.

Fankhauser, J. C., 1968: Thunderstorm-environment interactions revealed by chaff trajectories in mid troposphere. ESSA Tech. Memo ERLTM-NSSL-39, National Severe Storms Laboratory, Norman, Oklahoma, 14 pp.

_____, 1971: Thunderstorm-environment interactions determined from aircraft and radar observations. Mon. Wea. Rev., 99, 171-192.

Fujita, T., 1965: Formation and steering mechanisms of tornado cyclones and associated hook echoes. Mon. Wea. Rev., 93, 67-78.

_____, and H. Grandoso, 1968: Split of a thunderstorm into anticyclonic and cyclonic storms and their motion as determined from numerical model experiments. J. Atmos. Sci., 25, 416-439.

Goldman, J. L., 1966: The role of the Kutta-Joukowski force in cloud systems with circulation. ESSA Tech. Memo ERLTM-NSSL-27, National Severe Storms Laboratory, Norman, Oklahoma, 34 pp.

Jessup, E. A., 1972: Interpretations of chaff trajectories near a severe thunderstorm. Mon. Wea. Rev., 100, 653-661.

Kessler, E., 1970: Thunderstorms over Oklahoma 22 June 1969. Weatherwise, 23, 56-69.

Lemon, L. R., 1970: Formation and emergence of an anticyclonic eddy within a severe thunderstorm as revealed by radar and surface data. Preprints of Papers, Fourteenth Conf. on Radar Meteor., Tucson, Arizona, Amer. Meteor. Soc., 323-328.

Marwitz, J. D., 1972: The structure and motion of severe hailstorms. Part I: supercell storms. J. Appl. Meteor., 11, 166-179.

McMahon, H. J., D. P. Hester and J. G. Palferg, 1971: Vortex shedding from a turbulent jet in a crosswind. J. Fluid Mech., 48, 73-80.

Newton, C. W. and H. R. Newton, 1959: Dynamical interactions between large convective clouds and environment with vertical shear. J. Meteor., 16, 483-496.

Prandtl, L. and O. G. Tietjens, 1934: Applied Hydro- and Aeromechanics. Dover Publications, Inc., New York, 306 pp.

Rouse, H., 1946: Elementary Mechanics of Fluids. John Wiley and Sons, Inc., New York, 376 pp.

Sanders, L. D. and A. H. Webber, 1970: Evaluation of roughness lengths at the NSSL-WKY meteorological tower. ESSA Tech. Memo. ERLTM-NSSL-47, National Severe Storms Laboratory, Norman, Oklahoma, 24 pp.

Scorer, R. S., 1958: Natural Aerodynamics. Pergamon Press, New York, 312 pp.

Shmeter, S. M., 1970: Structure of fields of meteorological elements in a cumulonimbus zone. Translated by Israel Program for Scientific Translations, Jerusalem, 117 pp.

Ward, N. B., 1967: An effect of rotation on a buoyant convective column. Preprints of Papers, Fifth Conf. on Severe Local Storms, St. Louis, Missouri, Amer. Meteor. Soc., 368-373.

_____, 1968: Dynamic stability of a tornado cyclone. Preprints of Papers, Twelfth Conf. on Radar Meteor., Norman, Oklahoma, Amer. Meteor. Soc., 356-361.

Zimmerman, L. I., 1969: Atmospheric wake phenomena near the Canary Islands. J. Appl. Meteor., 8, 896-907.

APPENDIX A

OBJECTIVE SURFACE AND RADAR ANALYSES

Objective analyses of divergence, pressure, and wet-bulb potential temperature (in order as listed) are found immediately following the contoured radar echo (from Fig. 3, page 4). The objective analyses are on a fixed reference frame--the surface network analysis grid. The northwest and southeast sections of the analyses are not shown since no surface stations (or extrapolated data) exist there. The radar echo is tied to a smaller (but same scale) moving reference frame. The three representative surface stations (dots) included in other text figures are included in the analyses.

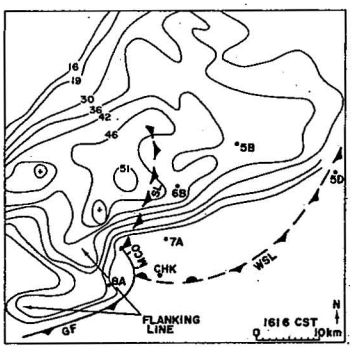
16
19
30
36
42
46
51
5B
6B
5D
7A
8A
CHK
WSL
FLANKING LINE
GF
1616 CST
N
0
10km

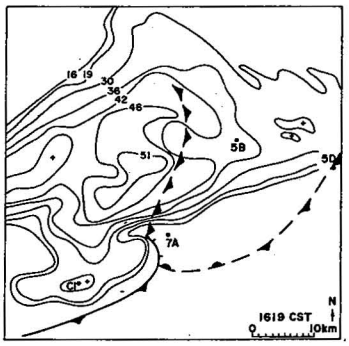
16 19
30
36
42
46
51
5B
5D
7A
GF
1619 CST
N
0
10km

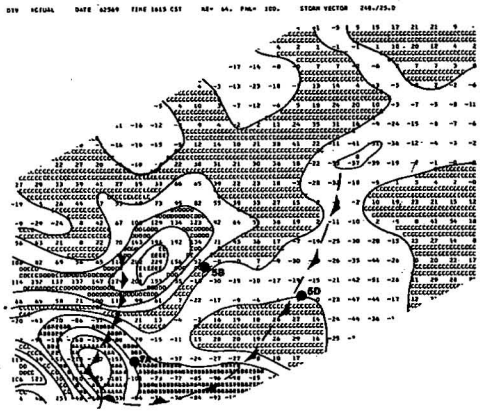

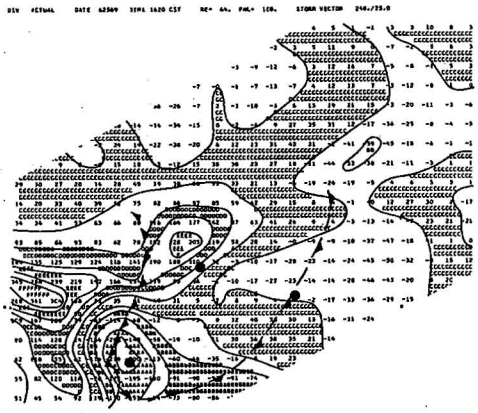

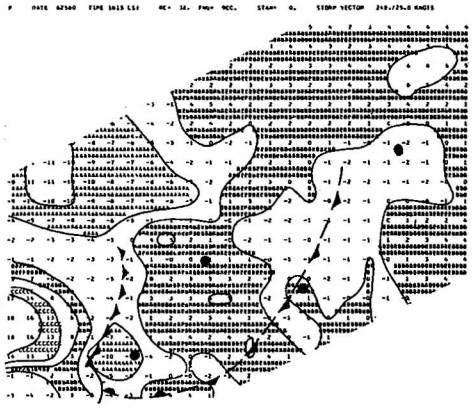

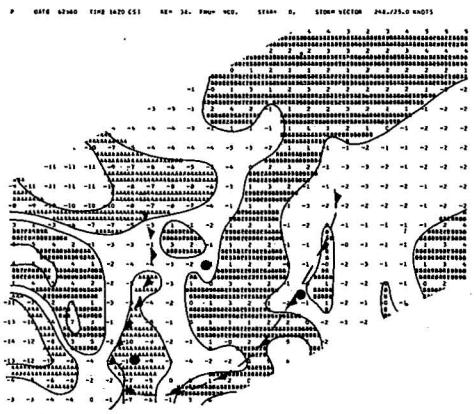

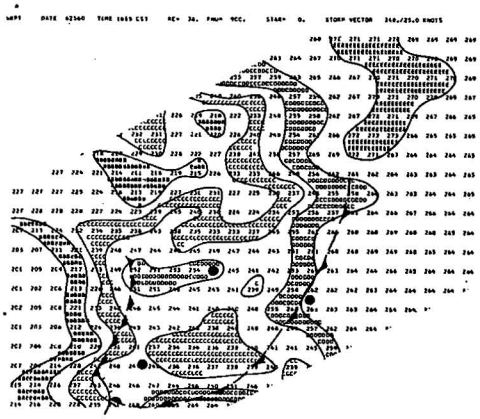

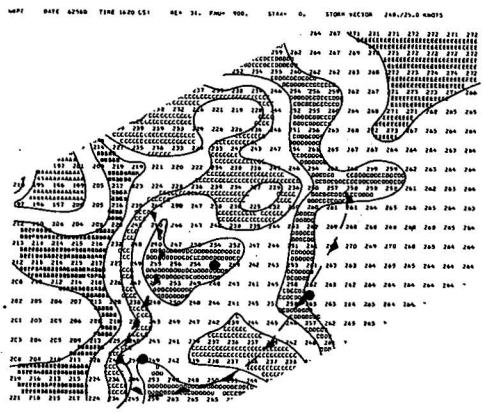

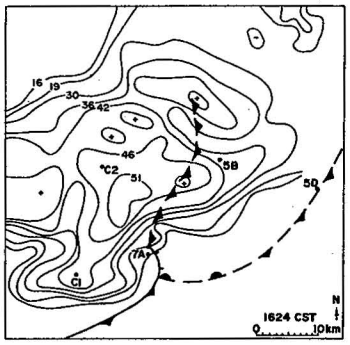
16
19
30
36
42
46
51
C2
C1
5B
5D
7A
1624 CST
N
0 10km

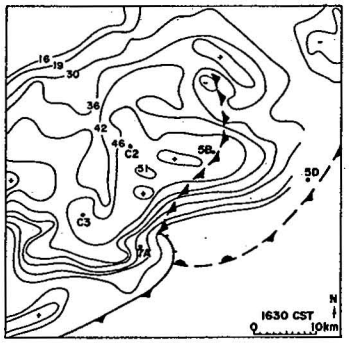
16
19
30
36
42
46
C2
C3
5B
5D
7A
1630 CST
N
0 10km

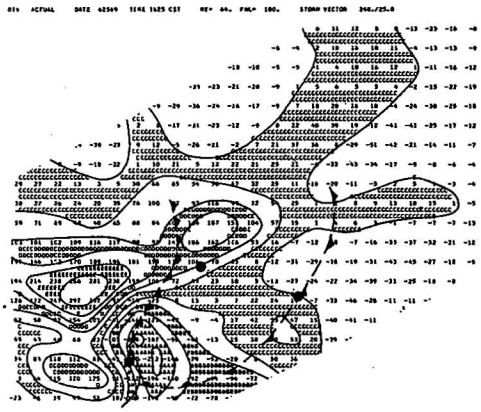

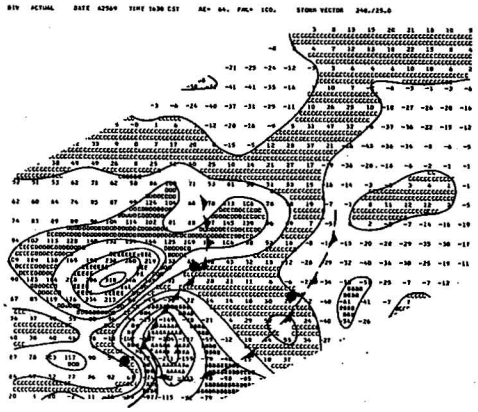

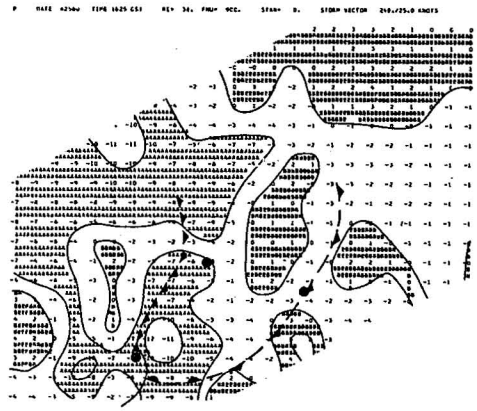

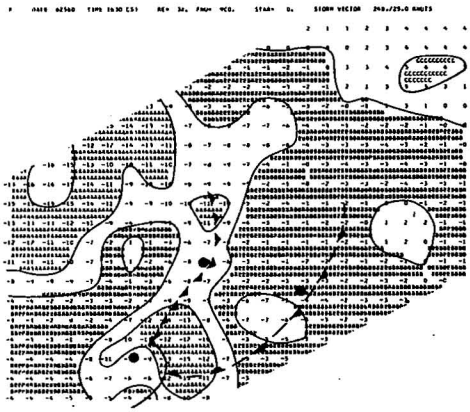

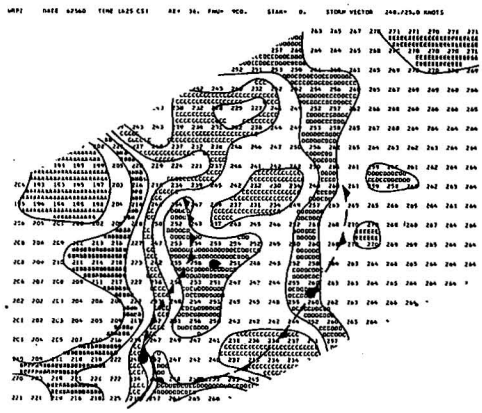

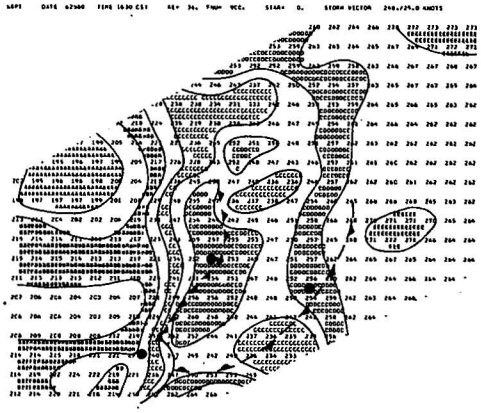

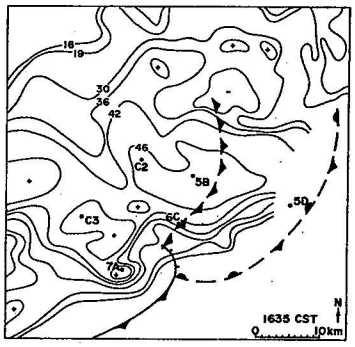
1635 CST
10km
N

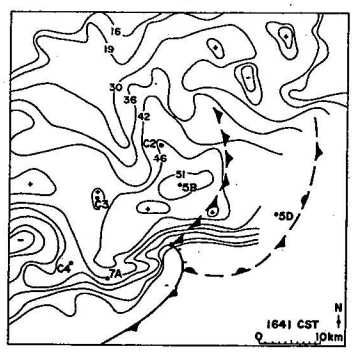
1641 CST
10km
N

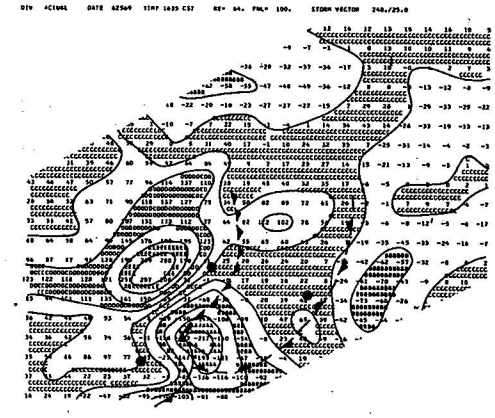

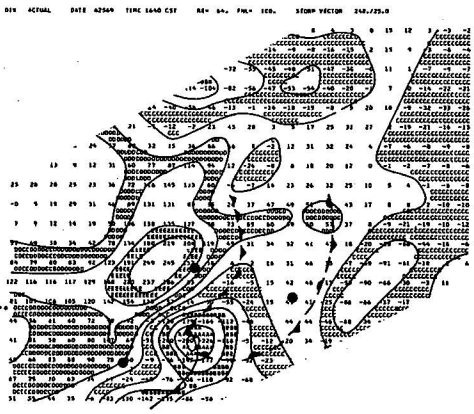

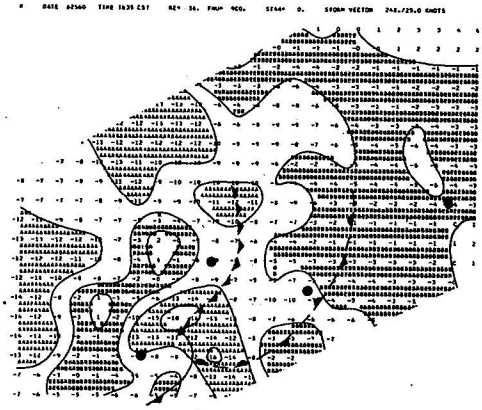

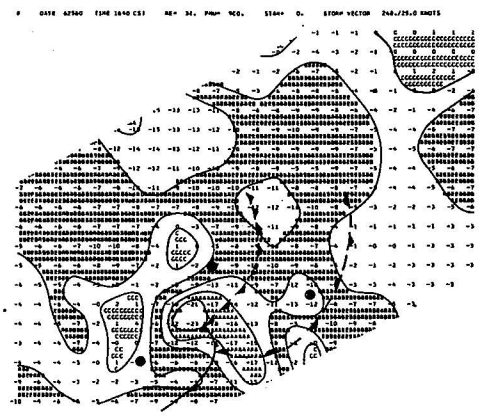

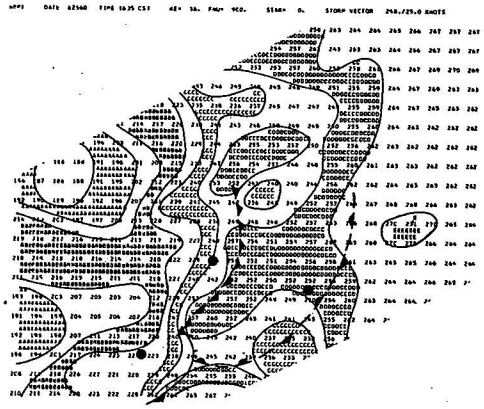

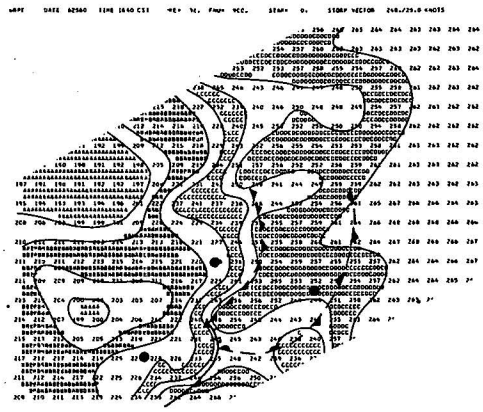

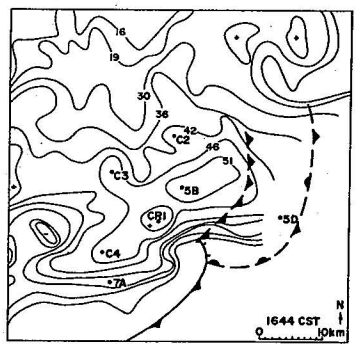
16
19
30
36
42
46
51
C2
C3
5B
CR1
5D
C4
7A
1644 CST
N
0
10km

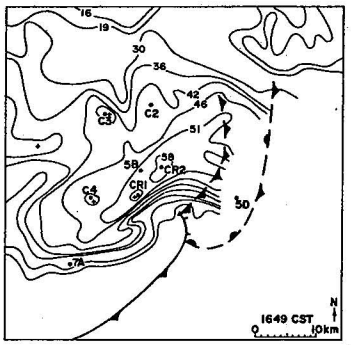
16
19
30
36
42
46
51
C2
C3
5B
CR2
CR1
C4
30
7A
1649 CST
N
0
10km

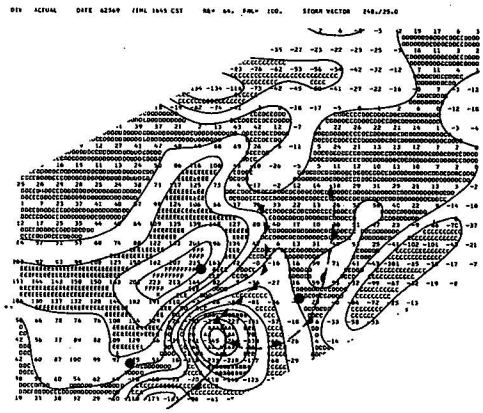

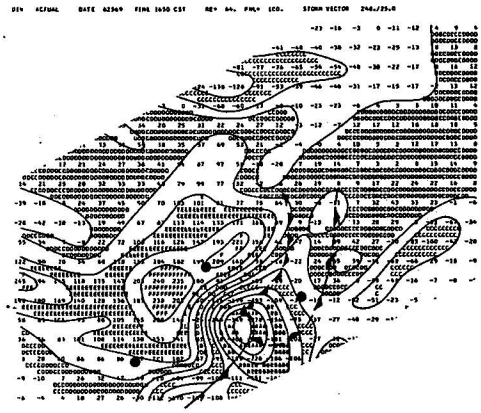

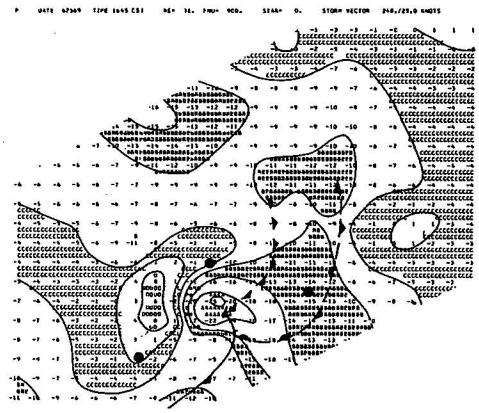

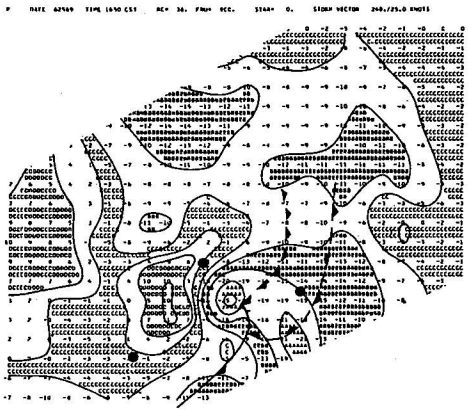

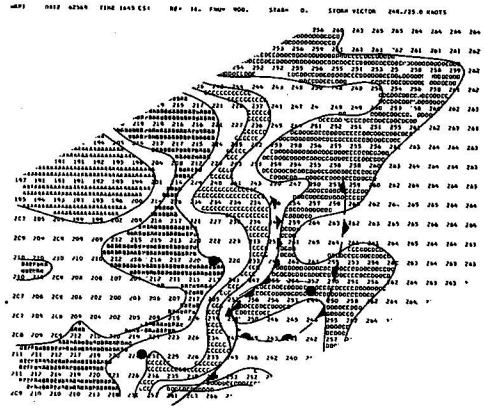

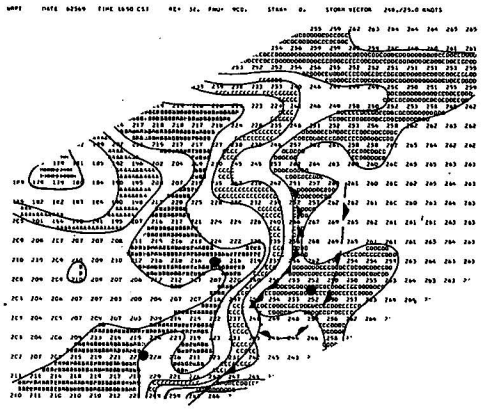

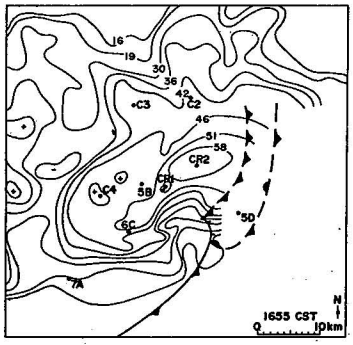
1655 CST
10km
N

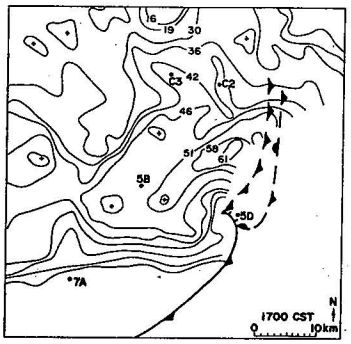
1700 CST
10km
N

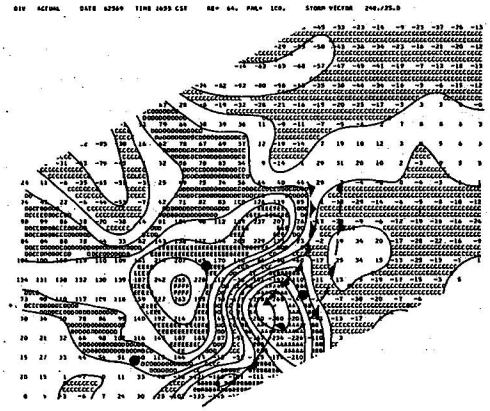

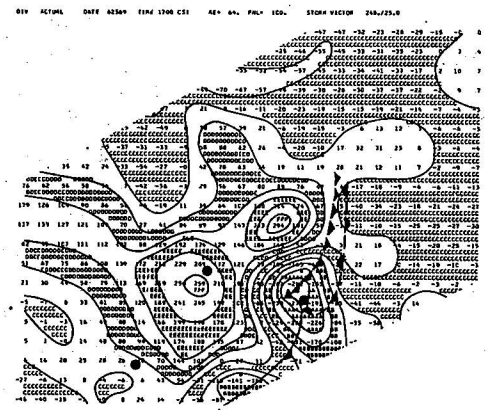

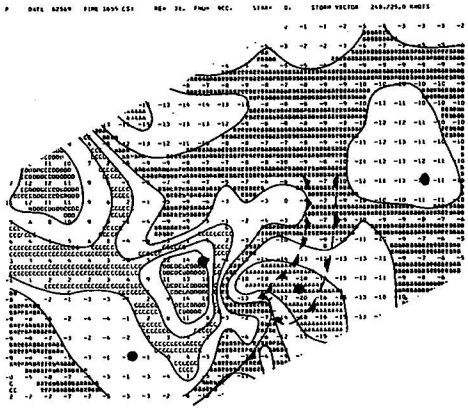

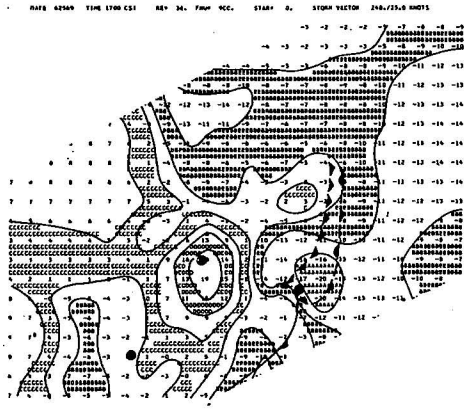

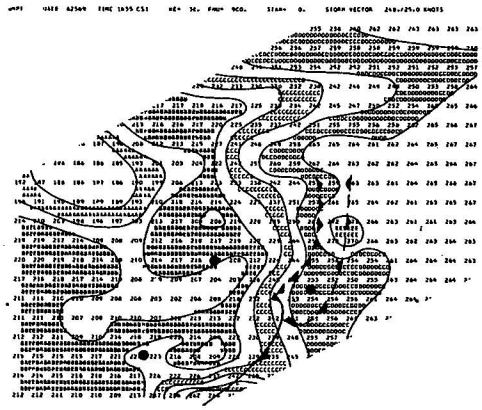

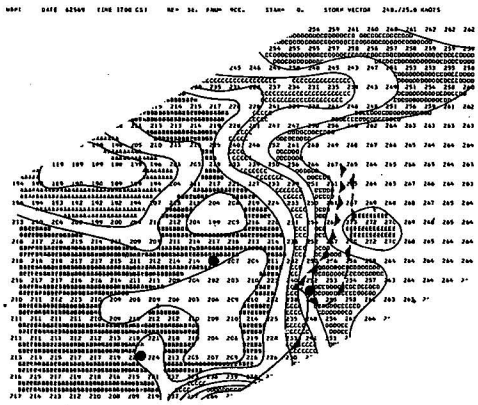

APPENDIX B

SURFACE DATA GRAPHS

Digital data extracted from analog traces (and corrected for station biases as explained in the first paper of this technical memorandum) were recorded on magnetic tape and presented here in graphical form. The time scale is in reversed chronological order so that it represents a space section with northeast on the graph right and southwest on the left. Station identifiers appear in the upper left oval (station locations are shown in Fig. 2 of the first paper). All plotted values are at 5-min intervals. Winds are 5-min averages while other parameters are instantaneous value. Wind vectors extend in the direction from which the winds are blowing and the scale at left indicates vector magnitude. For example, winds at station 1A are variable southerly with changing speeds while both north and south winds occur at station 4D. Maximum wind gusts during the 5 min preceding graph time are shown by a bar graph. Pressure (MB), temperature (F), relative humidity (%), accumulated rainfall (inches) and rainfall rate (inches/hour) are self explanatory. Missing data are so described except where only a brief break in a record occurs, as at station 5D, 1815-1830.

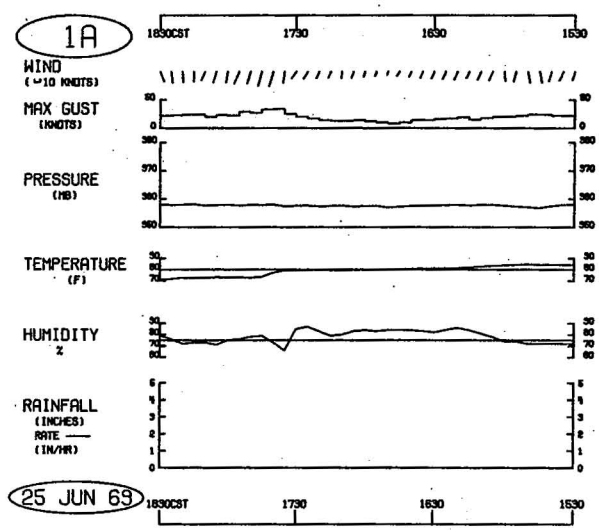
1A
1830CST
1730
1630
1530
WIND
(~10 KNOTS)
MAX GUST
(KNOTS)
PRESSURE
(MB)
TEMPERATURE
(F)
HUMIDITY
%
RAINFALL
(INCHES)
RATE
(IN/HR)
25 JUN 69

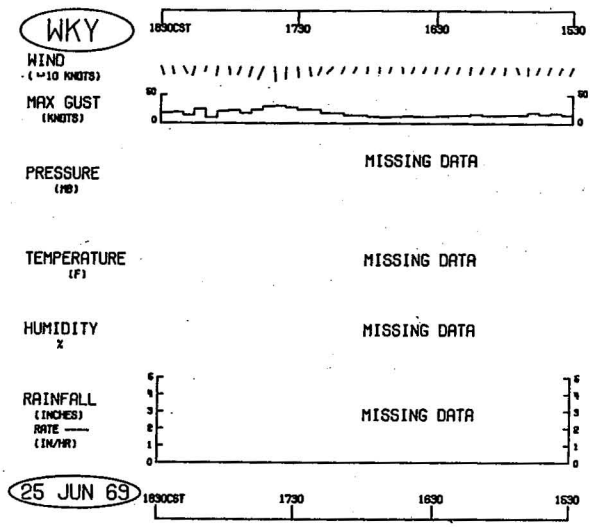
WKY
1830CST
1730
1630
1530
WIND
(~10 KNOTS)
MAX GUST
(KNOTS)
PRESSURE
(MB)
MISSING DATA
TEMPERATURE
(F)
MISSING DATA
HUMIDITY
%
MISSING DATA
RAINFALL
(INCHES)
RATE
(IN/HR)
MISSING DATA
25 JUN 69

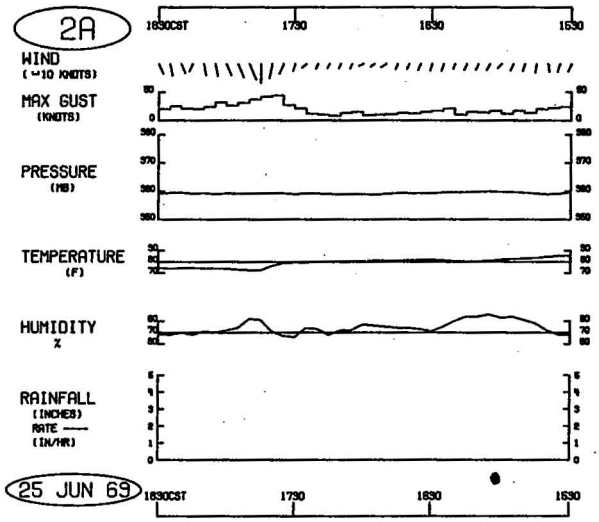
2A
1830CST
1730
1630
1530
WIND
(~10 KNOTS)
MAX GUST
(KNOTS)
PRESSURE
(MB)
TEMPERATURE
(F)
HUMIDITY
%
RAINFALL
(INCHES)
RATE
(IN/HR)
25 JUN 69

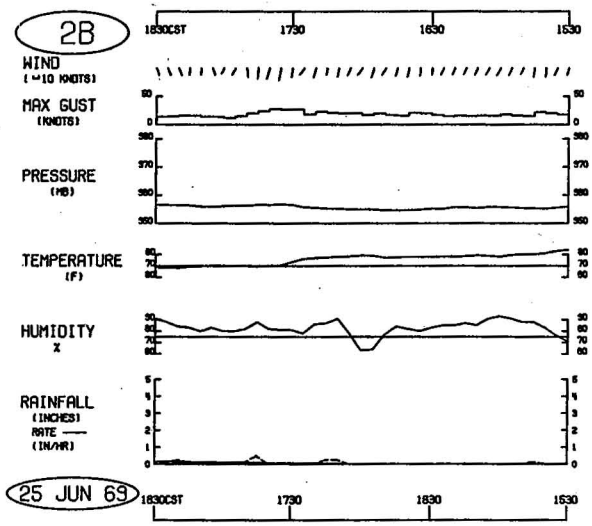
2B
1830CST
1730
1630
1530
WIND
(~10 KNOTS)
MAX GUST
(KNOTS)
PRESSURE
(MB)
TEMPERATURE
(F)
HUMIDITY
%
RAINFALL
(INCHES)
RATE
(IN/HR)
25 JUN 69

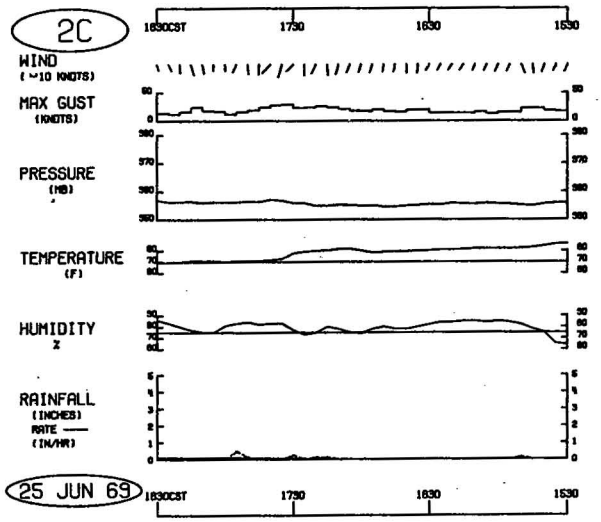
2C
1830CST
1730
1630
1530
WIND
(~10 KNOTS)
MAX GUST
(KNOTS)
PRESSURE
(MB)
TEMPERATURE
(F)
HUMIDITY
%
RAINFALL
(INCHES)
RATE
(IN/HR)
25 JUN 69

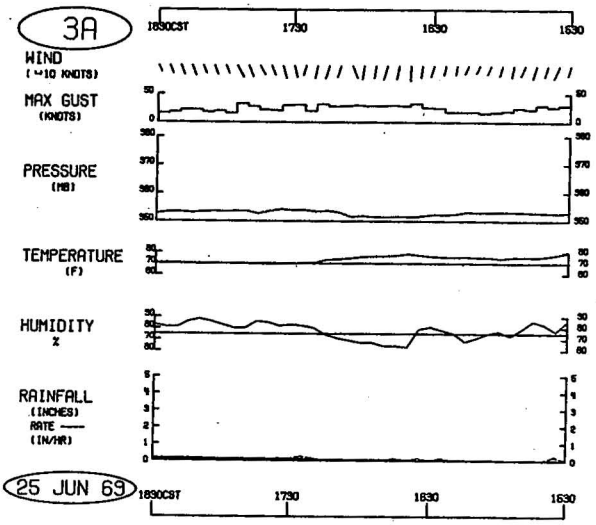
3A
1830CST
1730
1630
1530
WIND
(~10 KNOTS)
MAX GUST
(KNOTS)
PRESSURE
(MB)
TEMPERATURE
(F)
HUMIDITY
%
RAINFALL
(INCHES)
RATE
(IN/HR)
25 JUN 69

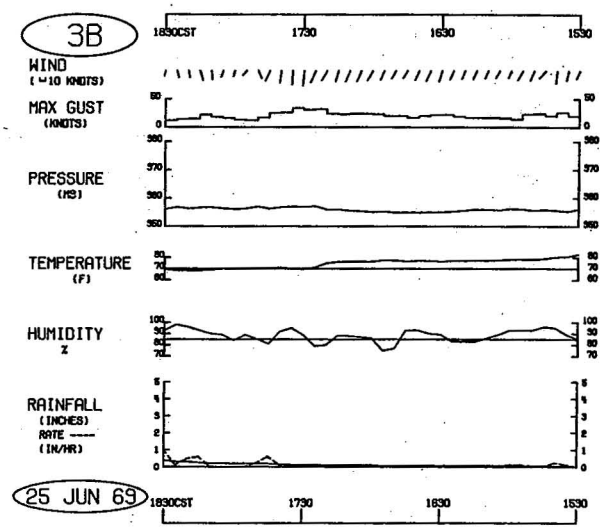
3B
1830CST
1730
1630
1530
WIND
(10 KNOTS)
MAX GUST
(KNOTS)
PRESSURE
(MB)
TEMPERATURE
(F)
HUMIDITY
%
RAINFALL
(INCHES)
RATE
(IN/HR)
25 JUN 69

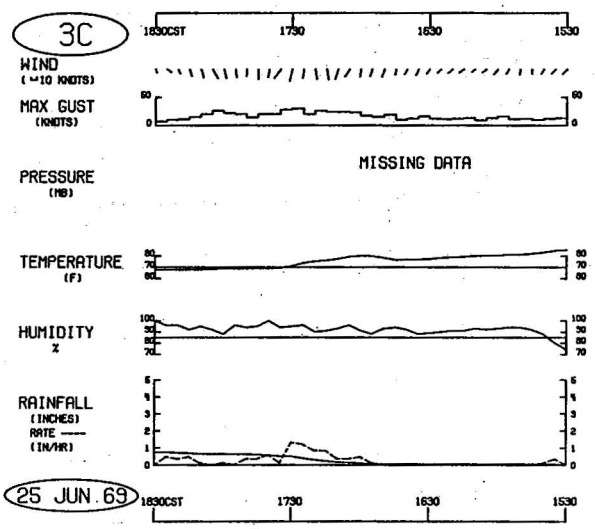
3C
1830CST
1730
1630
1530
WIND
(10 KNOTS)
MAX GUST
(KNOTS)
MISSING DATA
PRESSURE
(MB)
TEMPERATURE
(F)
HUMIDITY
%
RAINFALL
(INCHES)
RATE
(IN/HR)
25 JUN 69

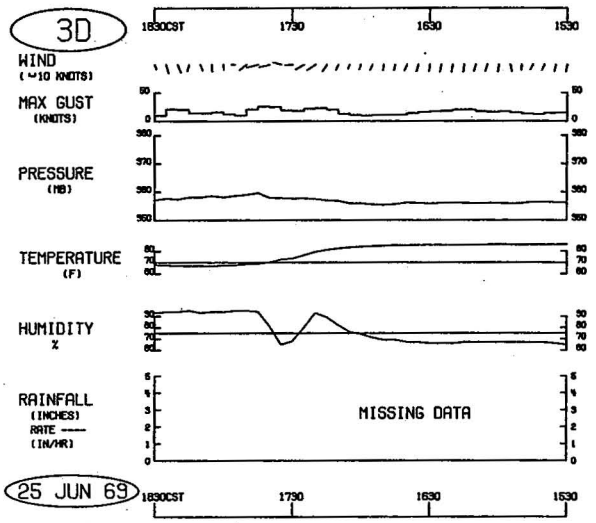
3D
1830CST
1730
1630
1530
WIND
(10 KNOTS)
MAX GUST
(KNOTS)
PRESSURE
(MB)
TEMPERATURE
(F)
HUMIDITY
%
RAINFALL
(INCHES)
RATE
(IN/HR)
MISSING DATA
25 JUN 69

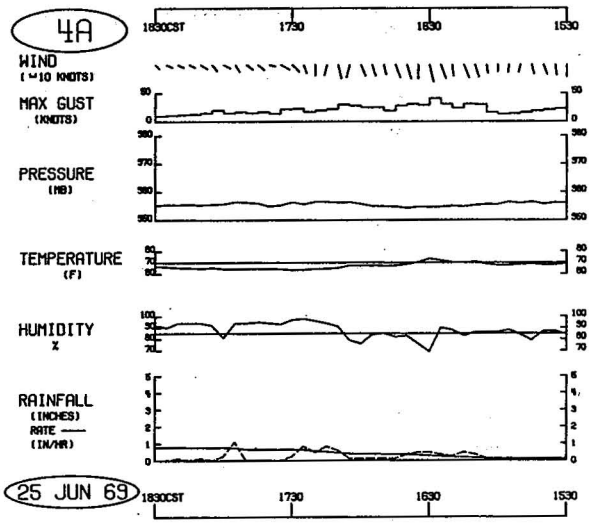
4A
1830CST
1730
1630
1530
WIND
(10 KNOTS)
MAX GUST
(KNOTS)
PRESSURE
(MB)
TEMPERATURE
(F)
HUMIDITY
%
RAINFALL
(INCHES)
RATE
(IN/HR)
25 JUN 69

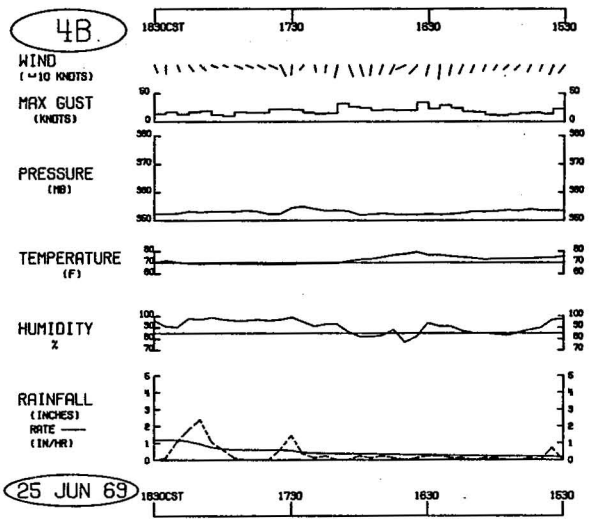
4B
1830CST
1730
1630
1530
WIND
(10 KNOTS)
MAX GUST
(KNOTS)
PRESSURE
(MB)
TEMPERATURE
(F)
HUMIDITY
%
RAINFALL
(INCHES)
RATE
(IN/HR)
25 JUN 69

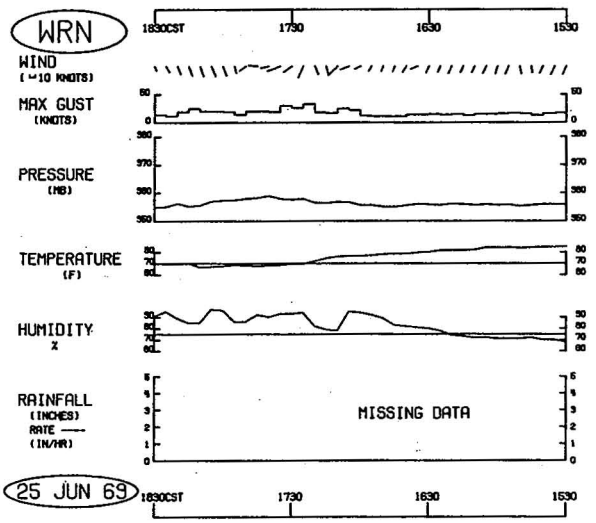
WRN
1830CST
1730
1630
1530
WIND
(10 KNOTS)
MAX GUST
(KNOTS)
PRESSURE
(MB)
TEMPERATURE
(F)
HUMIDITY
%
RAINFALL
(INCHES)
RATE
(IN/HR)
MISSING DATA
25 JUN 69

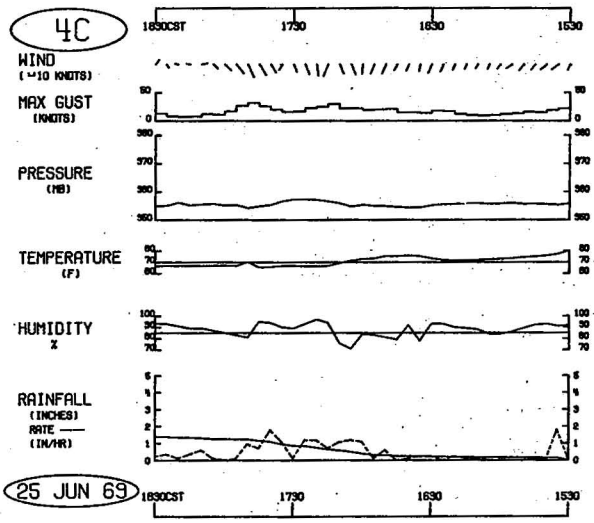
4C
1830CST
1730
1630
1530
WIND
(~10 KNOTS)
MAX GUST
(KNOTS)
PRESSURE
(MB)
TEMPERATURE
(F)
HUMIDITY
%
RAINFALL
(INCHES)
RATE
(IN/HR)
25 JUN 69

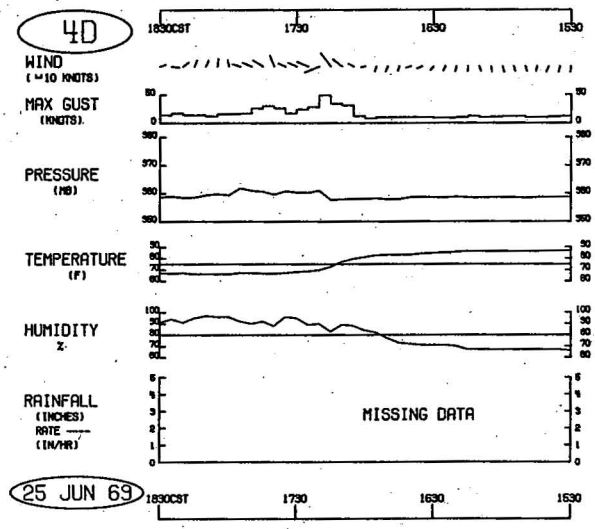
4D
1830CST
1730
1630
1530
WIND
(~10 KNOTS)
MAX GUST
(KNOTS)
PRESSURE
(MB)
TEMPERATURE
(F)
HUMIDITY
%
RAINFALL
(INCHES)
RATE
(IN/HR)
MISSING DATA
25 JUN 69

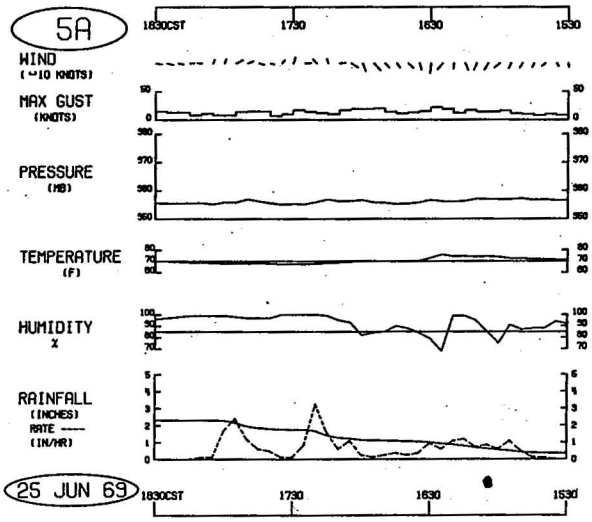
5A
1830CST
1730
1630
1530
WIND
(~10 KNOTS)
MAX GUST
(KNOTS)
PRESSURE
(MB)
TEMPERATURE
(F)
HUMIDITY
%
RAINFALL
(INCHES)
RATE
(IN/HR)
25 JUN 69

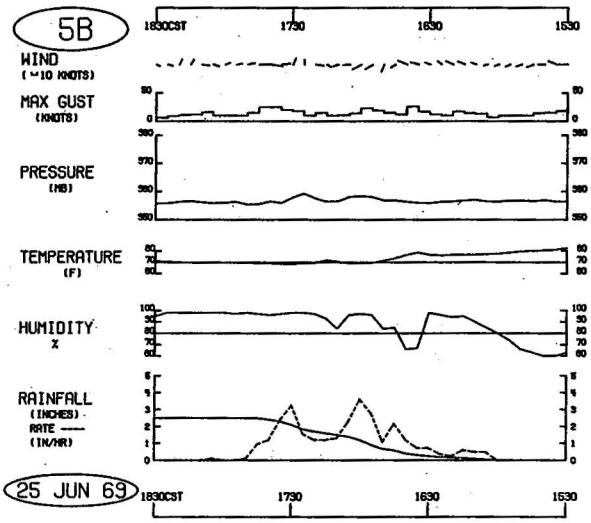
5B
1830CST
1730
1630
1530
WIND
(~10 KNOTS)
MAX GUST
(KNOTS)
PRESSURE
(MB)
TEMPERATURE
(F)
HUMIDITY
%
RAINFALL
(INCHES)
RATE
(IN/HR)
25 JUN 69

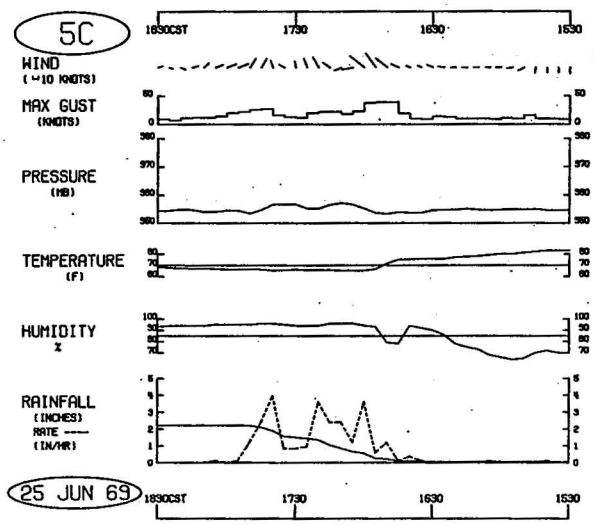
5C
1830CST
1730
1630
1530
WIND
(~10 KNOTS)
MAX GUST
(KNOTS)
PRESSURE
(MB)
TEMPERATURE
(F)
HUMIDITY
%
RAINFALL
(INCHES)
RATE
(IN/HR)
25 JUN 69

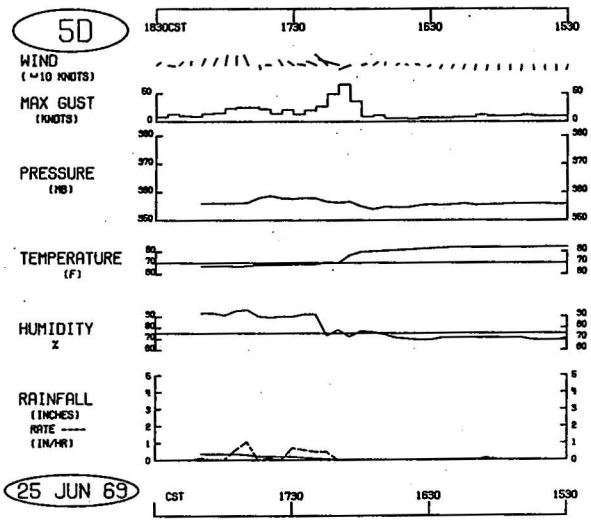
5D
1830CST
1730
1630
1530
WIND
(~10 KNOTS)
MAX GUST
(KNOTS)
PRESSURE
(MB)
TEMPERATURE
(F)
HUMIDITY
%
RAINFALL
(INCHES)
RATE
(IN/HR)
25 JUN 69
CST

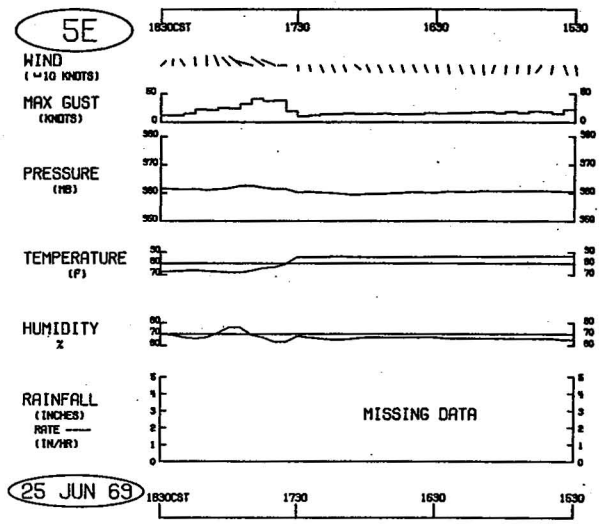
5E
1830CST
1730
1630
1530
WIND
(~10 KNOTS)
MAX GUST
(KNOTS)
PRESSURE
(MB)
TEMPERATURE
(F)
HUMIDITY
%
RAINFALL
(INCHES)
RATE
(IN/HR)
MISSING DATA
25 JUN 69

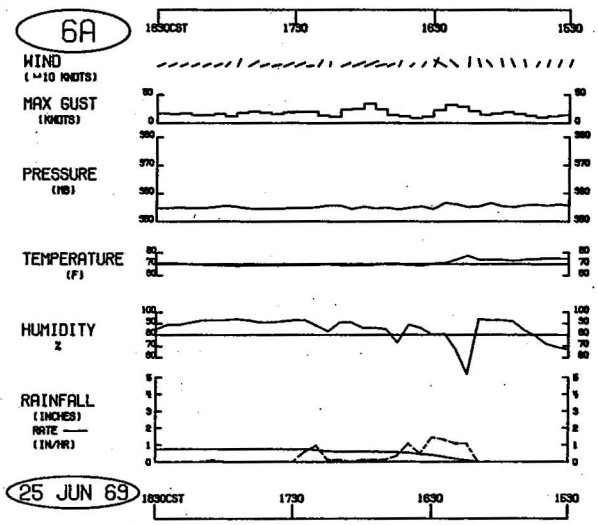
6A
1830CST
1730
1630
1530
WIND
(~10 KNOTS)
MAX GUST
(KNOTS)
PRESSURE
(MB)
TEMPERATURE
(F)
HUMIDITY
%
RAINFALL
(INCHES)
RATE
(IN/HR)
25 JUN 69

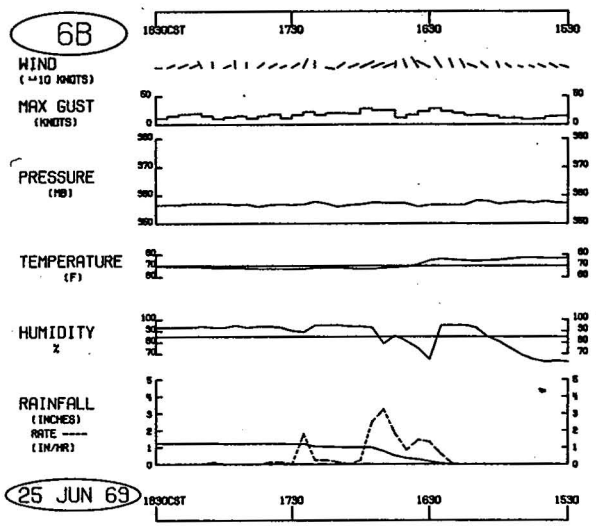
6B
1830CST
1730
1630
1530
WIND
(~10 KNOTS)
MAX GUST
(KNOTS)
PRESSURE
(MB)
TEMPERATURE
(F)
HUMIDITY
%
RAINFALL
(INCHES)
RATE
(IN/HR)
25 JUN 69

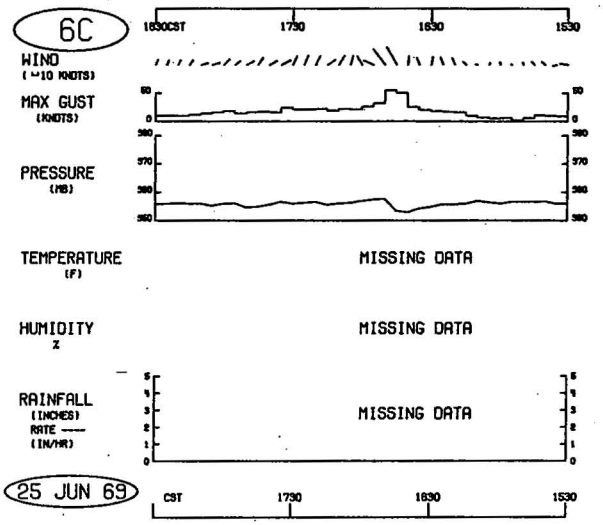
6C
1830CST
1730
1630
1530
WIND
(~10 KNOTS)
MAX GUST
(KNOTS)
PRESSURE
(MB)
TEMPERATURE
(F)
MISSING DATA
HUMIDITY
%
MISSING DATA
RAINFALL
(INCHES)
RATE
(IN/HR)
MISSING DATA
25 JUN 69
CST

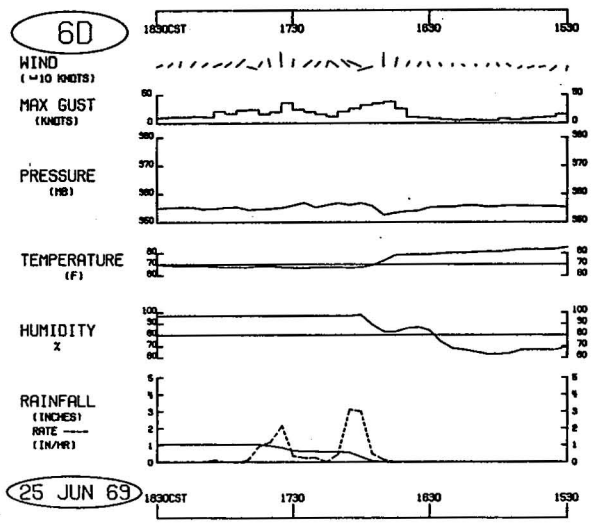
6D
1830CST
1730
1630
1530
WIND
(~10 KNOTS)
MAX GUST
(KNOTS)
PRESSURE
(MB)
TEMPERATURE
(F)
HUMIDITY
%
RAINFALL
(INCHES)
RATE
(IN/HR)
25 JUN 69

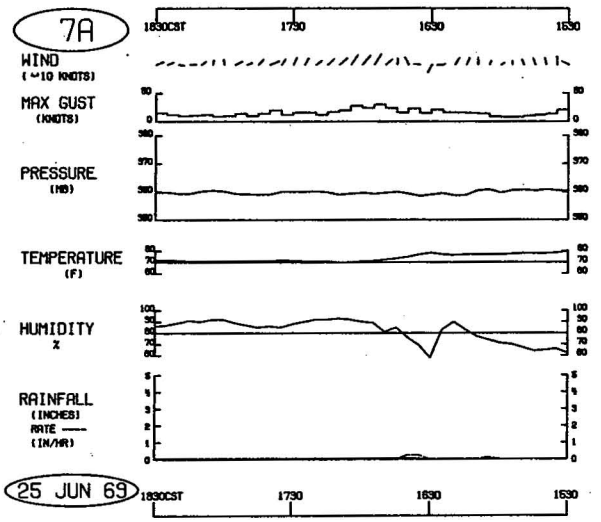
7A
1830CST
1730
1630
1530
WIND
(~10 KNOTS)
MAX GUST
(KNOTS)
PRESSURE
(MB)
TEMPERATURE
(F)
HUMIDITY
%
RAINFALL
(INCHES)
RATE
(IN/HR)
25 JUN 69

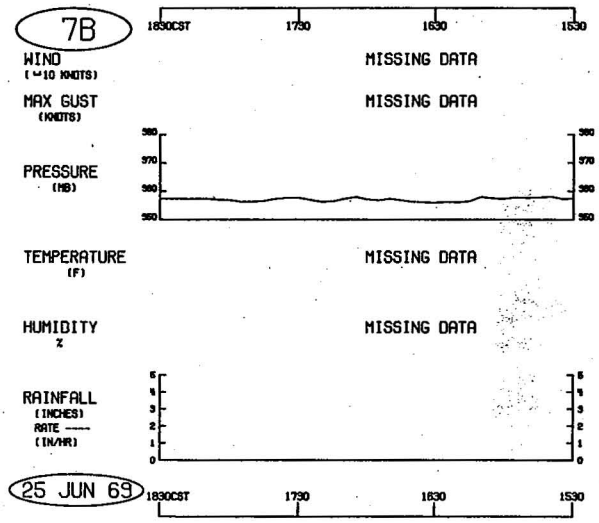
7B
1830CST
1730
1630
1530
WIND
(↑10 KNOTS)
MISSING DATA
MAX GUST
(KNOTS)
MISSING DATA
PRESSURE
(MB)
TEMPERATURE
(F)
MISSING DATA
HUMIDITY
%
MISSING DATA
RAINFALL
(INCHES)
RATE ——
(IN/HR)
25 JUN 69

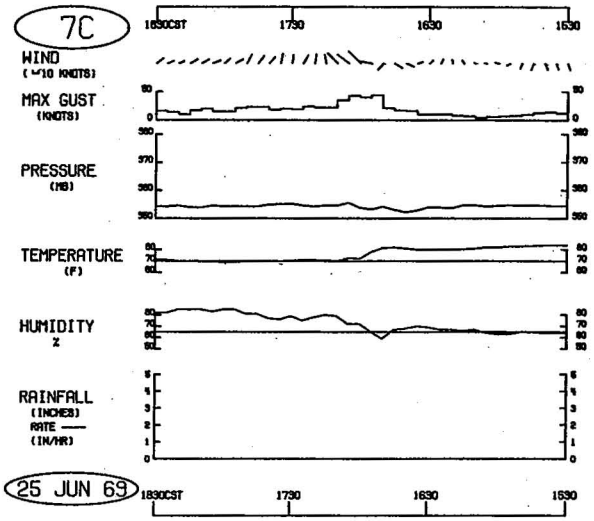
7C
1830CST
1730
1630
1530
WIND
(↑10 KNOTS)
MAX GUST
(KNOTS)
PRESSURE
(MB)
TEMPERATURE
(F)
HUMIDITY
%
RAINFALL
(INCHES)
RATE ——
(IN/HR)
25 JUN 69

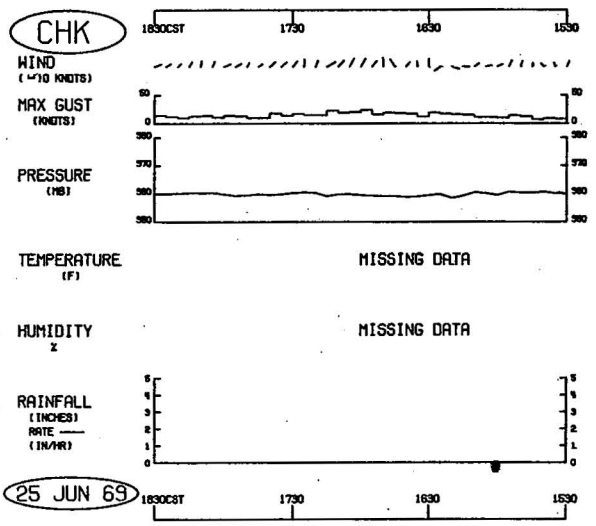
CHK
1830CST
1730
1630
1530
WIND
(↑10 KNOTS)
MAX GUST
(KNOTS)
PRESSURE
(MB)
TEMPERATURE
(F)
MISSING DATA
HUMIDITY
%
MISSING DATA
RAINFALL
(INCHES)
RATE ——
(IN/HR)
25 JUN 69

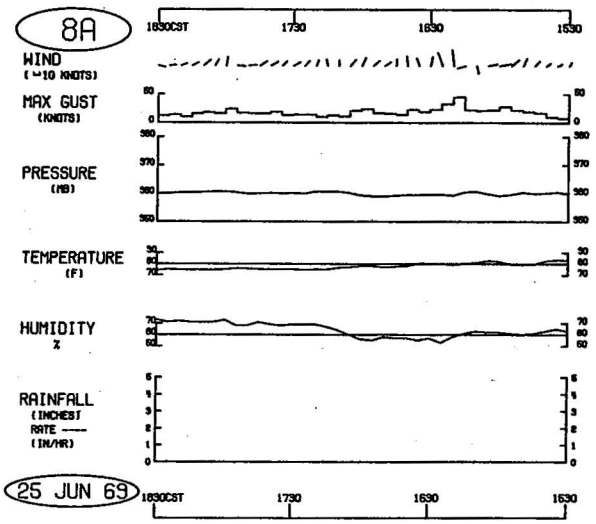
8A
1830CST
1730
1630
1530
WIND
(↑10 KNOTS)
MAX GUST
(KNOTS)
PRESSURE
(MB)
TEMPERATURE
(F)
HUMIDITY
%
RAINFALL
(INCHES)
RATE ——
(IN/HR)
25 JUN 69

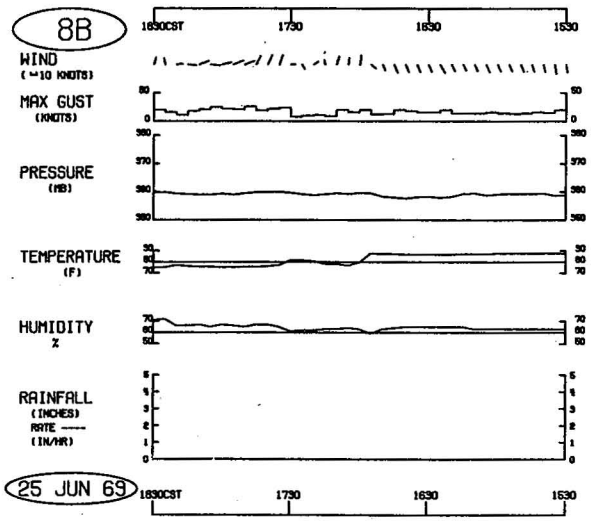
8B
1830CST
1730
1630
1530
WIND
(↑10 KNOTS)
MAX GUST
(KNOTS)
PRESSURE
(MB)
TEMPERATURE
(F)
HUMIDITY
%
RAINFALL
(INCHES)
RATE ——
(IN/HR)
25 JUN 69

APPENDIX C

OTHER WAKE VORTEX OCCURRENCES

NSSL has observed several storms to shed wake vortices. Of five well-documented cases, three are presented here. Data are incomplete in one case, and the fifth case is treated in the main body of the second paper.

In Fig. C1-A, the easternmost storm is the principal one studied in this technical memorandum. Immediately west of the first, a second storm produces a wake eddy as the interior bright core ($Z_e \geq 50$ dBZ) enlarges rapidly. Public reports at 1710 indicated "baseball" size hail and a funnel cloud with the storm. The storm altered its course 18° to the right after 1705.

Case B of Fig. C1 was attended by 4.5 cm hail during eddy shedding, increasing its rightward motion 17° by 1815. Kessler (1970) has discussed this and other 22 June 1969 storms.

Case C shows a recently documented wake vortex occurrence (18 June 1973) Three eddies were shed from this extremely intense storm. The first two (1613 and 1636) were short-lived and much less well-developed than the third (1704 - 1731). At 1613, near the southwest edge of the storm's core, hail up to 11 cm in diameter was falling. At 1643, 7 min following the second eddy signature, the first tornado occurred. During the most well developed wake vortex shedding (1704 - 1731), two tornadoes and 4 to 5 cm hail were observed. From 1613 - 1731, average storm movement was from 350° at 5.5 m sec^{-1}, or nearly 100° to the right of the mean winds.

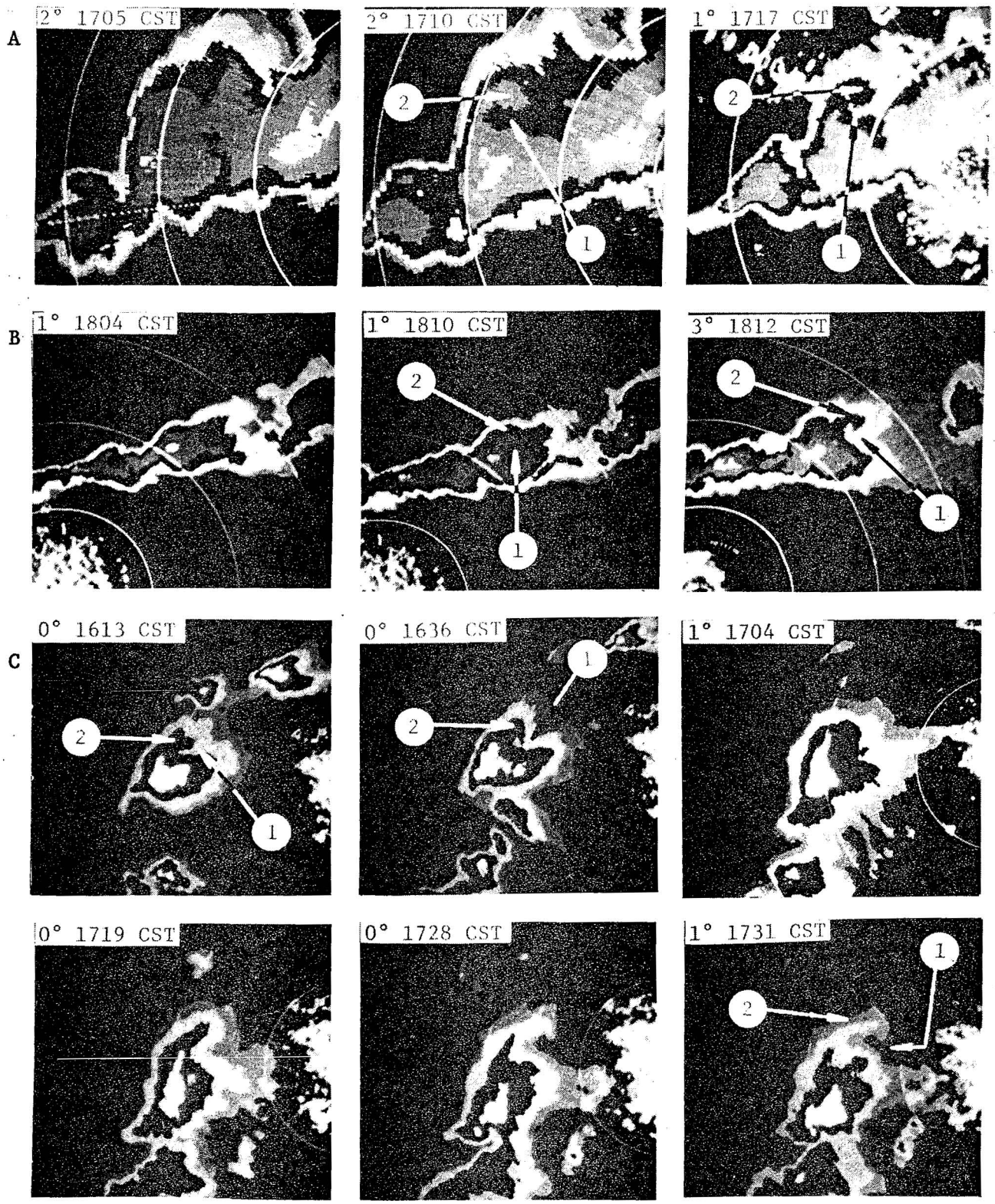

Figure C1. WSR-57 integrated log contour displays of eddy-shedding storms. (1) Low reflectivity intrusion, and (2) high reflectivity crescent. Range marks are 10 n mi (nm) in A except at 1717, where they are 20 n mi. Range marks are 20 n mi in B and 40 km in C.

NATIONAL SEVERE STORMS LABORATORY

The NSSL Technical Memoranda, beginning with No. 28, continue the sequence established by the U. S. Weather Bureau National Severe Storms Project, Kansas City, Missouri. Numbers 1-22 were designated NSSP Reports. Numbers 23-27 were NSSL Reports, and 24-27 appeared as subseries of Weather Bureau Technical Notes. These reports are available from the National Technical Information Service, Operations Division, Springfield, Virginia 22151, for $3.00, and a microfiche version for $0.95. NTIS numbers are given below in parentheses.

No. 1 National Severe Storms Project Objectives and Basic Design. Staff, NSSP. March 1961. (PB-168207)

No. 2 The Development of Aircraft Investigations of Squall Lines from 1956-1960. B. B. Goddard. (PB-168208)

No. 3 Instability Lines and Their Environments as Shown by Aircraft Soundings and Quasi-Horizontal Traverses. D. T. Williams. February 1962. (PB-168209)

No. 4 On the Mechanics of the Tornado. J. R. Fulks. February 1962. (PB-168210)

No. 5 A Summary of Field Operations and Data Collection by the National Severe Storms Project in Spring 1961. J. T. Lee. March 1962. (PB-165095)

No. 6 Index to the NSSP Surface Network. T. Fujita. April 1962. (PB-168212)

No. 7 The Vertical Structure of Three Dry Lines as Revealed by Aircraft Traverses. E. L. McGuire. April 1962. (PB-168213)

No. 8 Radar Observations of a Tornado Thunderstorm in Vertical Section. Ralph J. Donaldson, Jr. April 1962. (PB-174859)

No. 9 Dynamics of Severe Convective Storms. Chester W. Newton. July 1962. (PB-163319)

No. 10 Some Measured Characteristics of Severe Storms Turbulence. Roy Steiner and Richard H. Rhyne. July 1962. (N62-16401)

No. 11 A Study of the Kinematic Properties of Certain Small-Scale Systems. D. T. Williams. October 1962. (PB-168216)

No. 12 Analysis of the Severe Weather Factor in Automatic Control of Air Route Traffic. W. Boynton Beckwith. December 1962. (PB-168217)

No. 13 500-Kc./Sec. Sferics Studies in Severe Storms. Douglas A. Kohl and John E. Miller. April 1963. (PB-168218)

No. 14 Field Operations of the National Severe Storms Project in Spring 1962. L. D. Sanders. May 1963. (PB-168219)

No. 15 Penetrations of Thunderstorms by an Aircraft Flying at Supersonic Speeds. G. P. Roys. Radar Photographs and Gust Loads in Three Storms of 1961 Rough Rider. Paul W. J. Schumacher. May 1963. (PB-168220)

No. 16 Analysis of Selected Aircraft Data from NSSP Operations, 1962. T. Fujita. May 1963. (PB-168221)

No. 17 Analysis of Methods for Small-Scale Surface Network Data. D. T. Williams. August 1963. (PB-168222)

No. 18 The Thunderstorm Wake of May 4, 1961. D. T. Williams. August 1963. (PB-168223)

No. 19 Measurements by Aircraft of Condensed Water in Great Plains Thunderstorms. George P. Roys and Edwin Kessler. July 1966. (PB-173048)

No. 20 Field Operations of the National Severe Storms Project in Spring 1963. J. T. Lee, L. D. Sanders and D. T. Williams. January 1964. (PB-168224)

No. 21 On the Motion and Predictability of Convective Systems as Related to the Upper Winds in a Case of Small Turning of Wind with Height. James C. Fankhauser. January 1964. (PB168225)

No. 22 Movement and Development Patterns of Convective Storms and Forecasting the Probability of Storm Passage at a Given Location. Chester W. Newton and James C. Fankhauser. January 1964. (PB-168226)

No. 23 Purposes and Programs of the National Severe Storms Laboratory, Norman, Oklahoma. Edwin Kessler. December 1964. (PB-166675)

No. 24 Papers on Weather Radar, Atmospheric Turbulence, Sferics, and Data Processing. August 1965. (AD-621586)

No. 25 A Comparison of Kinematically Computed Precipitation with Observed Convective Rainfall. James C. Fankhauser. September 1965. (PB-168445).

No. 26 Probing Air Motion by Doppler Analysis of Radar Clear Air Returns. Roger M. Lhermitte. May 1966. (PB-170636)

No. 27 Statistical Properties of Radar Echo Patterns and the Radar Echo Process. Larry Armijo. May 1966. The Role of the Kutta-Joukowski Force in Cloud Systems with Circulation. J. L. Goldman. May 1966. (PB-170756)

No. 28 Movement and Predictablity of Radar Echoes. James Warren Wilson. November 1966. (PB-173972)

No. 29 Notes on Thunderstorm Motions, Heights, and Circulations. T. W. Harrold, W. T. Roach, and Kenneth E. Wilk. November 1966. (AD-644899)

No. 30 Turbulence in Clear Air Near Thunderstorms. Anne Burns, Terence W. Harrold, Jack Burnham, and Clifford S. Spavins. December 1966. (PB-173992)

No. 31 Study of a Left-Moving Thunderstorm of 23 April 1964. George R. Hammond. April 1967. (PB-174681)

No. 32 Thunderstorm Circulations and Turbulence from Aircraft and Radar Data. James C. Fankhauser and J. T. Lee. April 1967. (PB-174860)

No. 33 On the Continuity of Water Substance. Edwin Kessler. April 1967. (PB-175840)

No. 34 Note on the Probing Balloon Motion by Doppler Radar. Roger M. Lhermitte. July 1967. (PB-175930)

No. 35 A Theory for the Determination of Wind and Precipitation Velocities with Doppler Radars. Larry Armijo. August 1967. (PB-176376)

No. 36 A Preliminary Evaluation of the F-100 Rough Rider Turbulence Measurement System. U. O. Lappe. October 1967. (PB-177037)

No. 37 Preliminary Quantitative Analysis of Airborne Weather Radar. Lester P. Merritt. December 1967. (PB-177188)

No. 38 On the Source of Thunderstorm Rotation. Stanley L. Barnes. March 1968. (PB-178990)

No. 39 Thunderstorm - Environment Interactions Revealed by Chaff Trajectories in the Mid-Troposphere. James C. Fankhauser. June 1968. (PB-179659)

No. 40 Objective Detection and Correction of Errors in Radiosonde Data. Rex L. Inman. June 1968. (PB-180284)

No. 41 Structure and Movement of the Severe Thunderstorms of 3 April 1964 as Revealed from Radar and Surface Mesonetwork Data Analysis. Jess Charba and Yoshikazu Sasaki. October 1968. (PB-183310)

No. 42 A Rainfall Rate Sensor. Brian E. Morgan. November 1968. (PB-183979)

No. 43 Detection and Presentation of Severe Thunderstorms by Airborne and Ground-Based Radars: A Comparative Study. Kenneth E. Wilk, John K. Carter, and J. T. Dooley. February 1969. (PB-183572)

No. 44 A Study of a Severe Local Storm of 16 April 1967. George Thomas Haglund. May 1969. (PB-184-970)

No.45 On the Relationship Between Horizontal Moisture Convergence and Convective Cloud Formation. Horace R. Hudson. March 1970. (PB-191720)

No. 46 Severe Thunderstorm Radar Echo Motion and Related Weather Events Hazardous to Aviation Operations. Peter A. Barclay and Kenneth E. Wilk. June 1970. (PB-192498)

No. 47 Evaluation of Roughness Lengths at the NSSL-WKY Meteorological Tower. Leslie D. Sanders and Allen H. Weber. August 1970. (PB-194587)

No. 48 Behavior of Winds in the Lowest 1500 ft in Central Oklahoma: June 1966 - May 1967. Kenneth C. Crawford and Horace R. Hudson. August 1970.

No. 49 Tornado Incidence Maps. Arnold Court. August 1970. (COM-71-00019)

No. 50 The Meteorologically Instrumented WKY-TV Tower Facility. John K. Carter. September 1970. (COM-71-00108)

No. 51 Papers on Operational Objective Analysis Schemes at the National Severe Storms Forecast Center. Rex L. Inman. November 1970. (COM-71-00136)

No.52 The Exploration of Certain Features of Tornado Dynamics Using a Laboratory Model. Neil B. Ward. November 1970. (COM-71-00139)

No.53 Rawinsonde Observation and Processing Techniques at the National Severe Storms Laboratory. Stanley L. Barnes, James H. Henderson and Robert J. Ketchum. April 1971. (COM-71-00707)

No. 54 Model of Precipitation and Vertical Air Currents. Edwin Kessler and William C. Bumgarner. June 1971. (COM-71-00911)

No. 55 The NSSL Surface Network and Observations of Hazardous Wind Gusts. Operations Staff. June 1971. (COM-71-00910)

No. 56 Pilot Chaff Project at the National Severe Storms Laboratory. Edward A. Jessup. November 1971. (COM-72-10106)

No. 57 Numerical Simulation of Convective Vortices. Robert P. Davies-Jones and Glenn T. Vickers. November 1971. (COM-72-1026

No. 58 The Thermal Structure of the Lowest Half Kilometer in Central Oklahoma: December 9, 1966 - May 31, 1967. R. Craig Goff and Horace R. Hudson. July 1972. (COM-72-11281)

No. 59 Cloud-to-Ground Lightning Versus Radar Reflectivity in Oklahoma Thunderstorms. Gilbert D. Kinzer. September 1972. (COM-73-10050)

No. 60 Simulated Real Time Displays of Velocity Fields by Doppler Radar. L. D. Hennington and G. B. Walker. November 1972. (COM-73-10515)

No. 61 Gravity Current Model Applied to Analysis of Squall-Line Gust Front. Jess Charba. November 1972. (COM-73-10410)

No. 62 Mesoscale Objective Map Analysis Using Weighted Time-Series Observations. Stanley L. Barnes. March 1973. (COM-73-10781)

No. 63 Observations of Severe Storms on 26 and 28 April 1971. Charles L. Vlcek. April 1973. (COM-73-11200)

No. 64 Meteorological Radar Signal Intensity Estimation. Dale Sirmans and R. J. Doviak. September 1973. (COM-73-11923/2AS)

No. 65 Radiosonde Altitude Measurement Using Double Radiotheodolite Techniques. Stephan P. Nelson. September 1973. (COM-73-119

No. 66 The Motion and Morphology of the Dryline. Joseph T. Schaefer. September 1973. (COM-74-10043)

No. 67 Radar Rainfall Pattern Optimizing Technique. Edward A. Brandes. March 1974.

No . 68 The NSSL/WKY-TV Tower Data Collection Program: April - July 1972. R. Craig Goff and W. David Zittel. May 1974.

No. 69 Papers on Oklahoma Thunderstorms, April 29-30, 1970. Stanley L. Barnes, et al. May 1974

No. 70 Life Cycle of Florida Key's Waterspouts. Joseph H. Golden. June 1974

☆ U.S. GOVERNMENT PRINTING OFFICE 1974 - 677-233/1211 RE